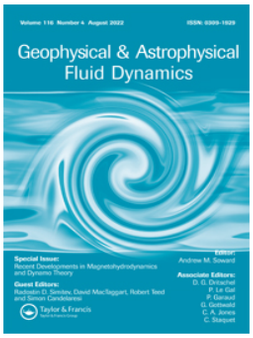

Taylor & Francis
Taylor & Francis Group

Geophysical & Astrophysical Fluid Dynamics

ISSN: (Print) (Online) Journal homepage: https://www.tandfonline.com/loi/ggaf20

An exact threshold for separator bifurcation

C. Prior & P. F. Wyper

To cite this article: C. Prior & P. F. Wyper (2022) An exact threshold for separator bifurcation, Geophysical & Astrophysical Fluid Dynamics, 116:4, 321-349, DOI: 10.1080/03091929.2022.2085696

To link to this article: https://doi.org/10.1080/03091929.2022.2085696

Published online: 21 Jun 2022.

GEOPHYSICAL & ASTROPHYSICAL FLUID DYNAMICS
2022, VOL. 116, NO. 4, 321–349
https://doi.org/10.1080/03091929.2022.2085696

Taylor & Francis
Taylor & Francis Group

An exact threshold for separator bifurcation

C. Prior and P. F. Wyper

Department of Mathematical Sciences, Durham University Upper Mountjoy Campus, Durham, UK

ABSTRACT

Reconnection involving magnetic separators is known to lead to the spontaneous generation of new separator pairs. In this work, we explore the bifurcation process for a system composed of a pair of null points with a joining separator. We begin with a simplified analytical model to derive the basic principles of bifurcation in this system and then consider models with more general separator curve geometry and generic localised null structure. We demonstrate that the maximum pairwise linking (net-winding) of the separator and the local fan plane always approaches a multiple of 0.25 just before bifurcation. Additionally, we show the integrated twisting along the separator (the field strength normalised parallel current) can be used to determine when this limit will definitely lead to bifurcation. We present step-by-step algorithms to assess how close such systems are to bifurcation.

ARTICLE HISTORY
Received 10 January 2022
Accepted 31 May 2022

KEYWORDS
Magnetic fields; magnetic topology; magnetic reconnection; separator bifurcation

1. Introduction

Magnetic reconnection, the process whereby magnetic field lines change their connectivity within regions of intense electric current, is a fundamental plasma process that underpins many astrophysical phenomena (Priest and Forbes 2000). Although a great deal of effort has been dedicated to understanding reconnection in two dimensions (2D) (e.g.Zweibel and Yamada 2009), in many scenarios, the three-dimensional (3D) nature of reconnection cannot be ignored and in fact in 3D reconnection is fundamentally different from 2D, occurring continuously throughout the volume of a current sheet (Hesse and Schindler 1988, Hornig and Priest 2003, Wyper and Hesse 2015). The key to understanding reconnection in three dimensions is understanding the 3D topological features of a magnetic field where current sheets naturally form; 3D null points, separators and Quasi-Separatrix Layers (e.g. Aulanier *et al.* 2005, Parnell *et al.* 2008, Priest and Pontin 2009), and how they evolve in response to reconnection within these current layers.

In this work, we focus on the problem of separator reconnection. Magnetic separators are field lines that connect two three-dimensional magnetic null points, lying at the intersection of each null's separatrix surface or "fan plane" (Priest and Titov 1996). Separators

CONTACT C. Prior christopher.prior@durham.ac.uk

are known to be preferential sites of current sheet formation and magnetic reconnection in astrophysical plasmas (e.g. Parnell *et al.* 2008). In the magnetosphere, separator reconnection plays an important role in dayside reconnection (Glocer *et al.* 2016). While in the solar corona interchange reconnection at separators may be an important source of the slow solar wind (e.g.Aslanyan *et al.* 2021) and could also be important in triggering certain coronal mass ejections (Wyper *et al.* 2021). Separator reconnection is also known to play a prominent role in many flux emergence experiments, occurring at the interface of emerging and pre-existing magnetic field (Parnell *et al.* 2010, MacTaggart and Haynes 2014).

Simulation and analytical studies have revealed that beyond some threshold apparently related to the current along a given separator, new pairs of separators can form via a bifurcation process (Haynes *et al.* 2007). As part of the process new flux domains are also formed bounded by the fan planes of each null and the new separators (Wilmot-Smith and Hornig 2011). These new flux domains can have important consequences. During dayside reconnection at the magnetopause these new flux domains in involved in flux transfer events, creating a direct pathway for particles in the solar wind to stream along field lines towards the Earth (Dorelli and Bhattacharjee 2009). In the context of interchange reconnection and the slow wind the formation of these new flux domains provides a direct route for closed field plasma to flow out along open field lines, feeding and modulating the slow solar wind (Pontin and Wyper 2015). Being able to predict the threshold at which the initial (and subsequent) bifurcations occur would, therefore, be beneficial in understanding these dynamic events.

The 3D null points that separator field lines connect also undergo a similar bifurcation process, with nulls forming or annihilating in pairs. Being point structures nulls can be well characterised by the their local behaviour. In Parnell *et al.* (1996) the linear structure of 3D nulls was fully characterised via the eigenvalues and eigenvectors of the Jacbobian matrix of the magnetic field vector around the null point. The null bifurcation process is inherently nonlinear at the point of bifurcation (Priest *et al.* 1996), however their linear behaviour can still capture the behaviour on either side of the transition (e.g. Wyper and Pontin 2014, figure 3). Separators are, however, non-local structures and although previous studies have considered (via the Jacobian) the linear behaviour of the in-plane components normal to the separator, showing a transition from hyperbolic to elliptical local structure along the separator (Parnell *et al.* 2010), no generic condition for bifurcation has been constructed. Nevertheless, the fact that separator pairs are known to form and annihilate along the curve of a pre-existing separator suggests this behaviour can be captured and quantified by linearising the magnetic field about this curve while still keeping the nonlinear behaviour of the field *along* the separator. This approach preserves the non-local nature of the field and is the approach we take initially in this work. In what follows we apply this methodology to the analytical model of separator bifurcation presented by Wilmot-Smith and Hornig (2011), before exploring more general field examples. Our analysis shows that the separator bifurcation process is related to a fixed increase in field line linking in the vicinity of the separator. Based on this we introduce two complimentary measures for assessing how close to bifurcation a given pre-existing separator is.

2. The baseline model

A simplified model for a null-separator magnetic structure $\boldsymbol{B}_n$ introduced in Wilmot-Smith and Hornig (2011) can be represented in a Cartesian coordinate system as

$$\boldsymbol{B}_n = \frac{b_0}{L^2}[x(z-3z_0)\hat{\boldsymbol{x}} + y(z+3z_0)\hat{\boldsymbol{y}} + (z_0^2 - z^2 + x^2 + y^2)\hat{\boldsymbol{z}}], \tag{1}$$

where b_0 and L^2 a give the characteristic strength and length scaling of the field, respectively. The null points of this field, $\boldsymbol{B} = \boldsymbol{0}$, are at $x = y = 0, z = \pm z_0$. The *separator* is the field line following the curve $x = y = 0, z \in (-z_0, z_0)$, which joins these null points. The field $\boldsymbol{B}_n$ is divergence-free, but it has current (a non-vanishing curl) away from the nulls and separator lines. The null Jacobians are (up to a factor b_0/L^2)

$$\begin{pmatrix} -4z_0 & 0 & 0 \\ 0 & 2z_0 & 0 \\ 0 & 0 & 2z_0 \end{pmatrix} \quad \text{and} \quad \begin{pmatrix} -2z_0 & 0 & 0 \\ 0 & 4z_0 & 0 \\ 0 & 0 & -2z_0 \end{pmatrix}.$$

So (up to a scaling factor) the local field structure of these nulls is

$$\boldsymbol{B}_0^{-z_0} = -2x\hat{\boldsymbol{x}} + y\hat{\boldsymbol{y}} + (z - z_0)\hat{\boldsymbol{z}} \qquad \text{and} \qquad \boldsymbol{B}_0^{z_0} = -x\hat{\boldsymbol{x}} + 2y\hat{\boldsymbol{y}} - (z - z_0)\hat{\boldsymbol{z}}.$$

As shown in figure 1(a), this means the spine field lines point inwards towards the null at $-z_0$. Field lines traced forward from a point just in front of this null, $z = -z_0 + \delta$ then trace towards the other null at $z = z_0$, with their z coordinate tending monotonically towards the plane $z = z_0$. The spine field lines of the null at $z = z_0$ are directed away from the null towards $s^+ = (0, \infty, z_0)$ and $s^- = (0, -\infty, z_0)$. Any field lines traced forward from just in-front of the $z = -z_0$ null, with a **negative** y coordinate, will, as its z coordinate increases, tend towards s^-, this is indicated by the Red field lines in figure 1(a). Those for which $y > 0$ will tend towards s^+ and are shown in blue in figure 1(a). While those with $y = 0$ form part of the fan plane of the null at $z = z_0$. This directed topology, splitting towards s^+ and s^- will be crucial in the development of additional separator structures, which arise as we add current to the model in what follows.

2.1. Twist induced reconnection

To model the reconnective process (Wilmot-Smith and Hornig 2011) added an additional twisting field $\boldsymbol{B}_t$ centred at $z = 0$ and given by the expression

$$\boldsymbol{B}_t = \frac{2b_1}{m}(-y\hat{\boldsymbol{x}} + x\hat{\boldsymbol{y}}) \exp\left(-\frac{(x^2+y^2)}{m^2} - \frac{z^2}{l^2}\right). \tag{2}$$

The parameter b_1 controls the maximum twist rate of the field, m controls the decay of the twisting radially away from the separatrix line (this was labelled a in Wilmot-Smith and Hornig 2011) and l determines the localisation of the twisting along the separatrix line. The parameters l and m are typically to be chosen so that the twisting is localised in-between the two null points, resistive simulations of the evolution of such structures indicate this often occurs (Stevenson *et al.* 2015). As discussed in Wilmot-Smith and Hornig (2011), one can

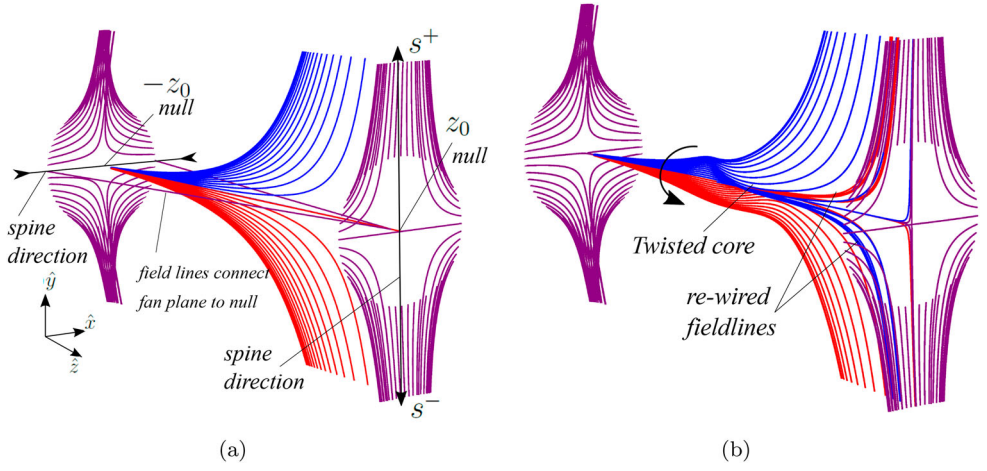

Figure 1. Illustrations of the field line structure of the standard null-separator structure used to derive the basic result. Panel (a) shows field lines of the field $\boldsymbol{B}_n$. The purple field lines indicate the spine/fan plane structure of the two null points at $\pm z_0$. The spine lines are shown to tend in towards the null at $z = -z_0$. Field lines in the fan plane just in front of null tend towards the null point at $z = z_0$. At the $z = z_0$ null the spine tends towards two limits s^+ and s^-. The blue field lines start at $z = -z_0 + \delta$, just in front of the null with a positive y coordinate, the red field lines have a negative y coordinate. They tend respectively to the spline limits s^+ and s^-. In panel (b) we see example field lines of $\boldsymbol{B}_n + \boldsymbol{B}_t$ with the additional twisted field core centred at $z = 0$. The positive chirality of the twisting is indicated. These field lines have the same start points as those shown in (a). The effect of the twisted at the core is shown to reconnect blue lines to s^+ and red lines to s^-, as indicated. (Colour online)

think of the evolution of the field as b_1 is increased as being a kinematic time-dependent reconnective evolution with b_1 parameterising time.

An indication of the effect of this twisting on the field line topology of the sum $\boldsymbol{B}_n + \boldsymbol{B}_t$ due to a non-zero b_1 is given in figure 1(b). The twist at the centre of the separator means that there is an alteration of the connectivity of the fan planes of the two nulls. After twisting, a subset of field lines traced forward from near the null at $-z_0$, with a negative y coordinate, develop a positive y coordinate value at some $z < z_0$, due to being twisted around the separator, and end up being directed to s^+. That is, they have reconnected across the fan plane of the null at $z = z_0$. The example shown in the figure has a positive twisting chirality $b_1 > 0$, if a negative twist is applied ($b_1 < 0$) then the same altering of connectivity will occur, *i.e.* negative y initial points to s^+ and vice versa. But, by contrast, the blue (positive initial y) field lines would approach s^- with positive x coordinate rather than a negative one (which is the case for the positive twisting figure).

2.1.1. Using polar coordinates to quantify the reconnection.

This reconnection occurs for any positive b_1 but for certain critical values, we will see it leads to separator bifurcation and a distinct topological change. To understand the bifurcation process, we introduce a cylindrical coordinate system (r, θ, z), centred on the separator at $r = 0$ and with $\theta = \arctan(y/x)$ meaning the branch cut in θ is at $x = 0$.

Thus $\theta < \pi$ corresponds to $y > 0$ and, for $b_1 = 0$ (no twist) all field lines with start points such that $0 < \theta_0 < \pi$ and $z > -z_0$ tend towards s^+ and all field lines with start

points such that $\pi < \theta_0 < 2\pi$ (and $z > -z_0$) tend to s^-. The field lines whose initial angles are $\theta_0 = 0$ and $\theta_0 = \pi$ tend to the null at z_0 as they lie in the fan plane of the z_0 null point (figure 1(a)). As b_1 is increased the twisting induces a map

$$\theta(z) \to \theta(z) + \phi(r, b_1, z).$$

The function $\phi(r, b_1, z)$ represents the rotation of the field line around the separator line. It is zero for $b_1 = 0$ and increases monotonically with b_1. The r dependence is due to the fact that the twisting decays with radius from the initial separator. We can characterise the function ϕ more precisely as follows. The field line equation for field lines in between the two nulls is

$$\frac{\mathrm{d}\boldsymbol{r}}{\mathrm{d}z} = \frac{\boldsymbol{B}}{B_z}.$$

If we write $x = r\cos\theta$ and $y = r\sin\theta$ and insert this into $\boldsymbol{B}_0 + \boldsymbol{B}_t$ (see (1) and (2)), then the component parts of these equations become

$$\begin{aligned} \frac{\mathrm{d}\theta}{\mathrm{d}z} &= \frac{B_\theta}{rB_z} = \frac{(3b_0/L^2)z_0\sin(2\theta) + (2b_1/m)\exp(-r^2/a^2 - z^2/l^2)}{(b_0/L^2)(z_0^2 - z^2 + r^2)}, \\ \frac{\mathrm{d}r}{\mathrm{d}z} &= \frac{B_r}{B_z} = \frac{r(z - 3z_0\cos(2\theta))}{z_0^2 - z^2 + r^2}. \end{aligned} \tag{3}$$

If $b_1 = 0$ we obtain the form of the functions $(r(z), \theta(z))$ from some initial condition $z = -z_0 + \delta$ by solving these equations (numerically in this case). The function ϕ results from solving the same equations with $b_1 \neq 0$ and comparing to the $b_1 = 0$ case, but it is not simple to characterise as this is a coupled nonlinear system.

2.1.2. Rotation about the initial separator

Some insight into this system can be obtained by considering the rotation about the separator when $r = \epsilon \ll 1$. In this case we can expand (3) in r, about $r = 0$, to find that the θ equation decouples from r at leading order

$$\frac{\mathrm{d}\theta}{\mathrm{d}z} = \frac{3z_0\sin(2\theta) + (2b_1/m)\exp(-z^2/l^2)}{z_0^2 - z^2}. \tag{4}$$

This will be the crucial equation in what follows. Consider first the case for which $b_1 = 0$. We label the initial condition $z_i = -z_0 + \delta$, where $\delta > 0$. If $\theta(z_i) = 0, \pi/2, \pi$ or $3\pi/2$, this equation has a fixed point representing the field lines in the fan plane of the $-z_0$ null ($\theta(z_i) = \pi/2, 3\pi/2$), which also correspond the to the angle of the spine curves of the z_0 null. If $\theta(z_i) = 0, \pi$ then the field line is in the fan plane of the z_0 null (and aligned with spine direction of the $-z_0$ null). Various plots in figure 2(a) illustrate the general behaviour of the system. If $\theta(z_i) \in (0, \pi/2)$ then $\sin(2\theta)$ is positive and θ will increase with z. Then, since the denominator tends to zero as $z \to z_0$, the rate of increase blows up so that θ will tend to the stable fixed point $\theta = \pi/2$. A similar argument for $\theta(z_i) \in (3\pi/2, 2\pi)$ has $\theta(z)$ tending to $3\pi/2$ as $z \to z_0$, so $\theta = 0$ is an unstable fixed point. By a similar argument, we see $\theta = \pi$ is an unstable fixed point with all $\theta(z_i) \in (\pi/2, \pi)$ tending towards $\pi/2$ (a stable fixed point) and all $\theta(z_i) \in (\pi, 3\pi/2)$ tending to the fixed point $\theta = 3\pi/2$. This behaviour is seen in figure 1(a) where the field lines either tend to s^+ ($\theta = \pi/2$) or s^- ($\theta = 3\pi/2$).

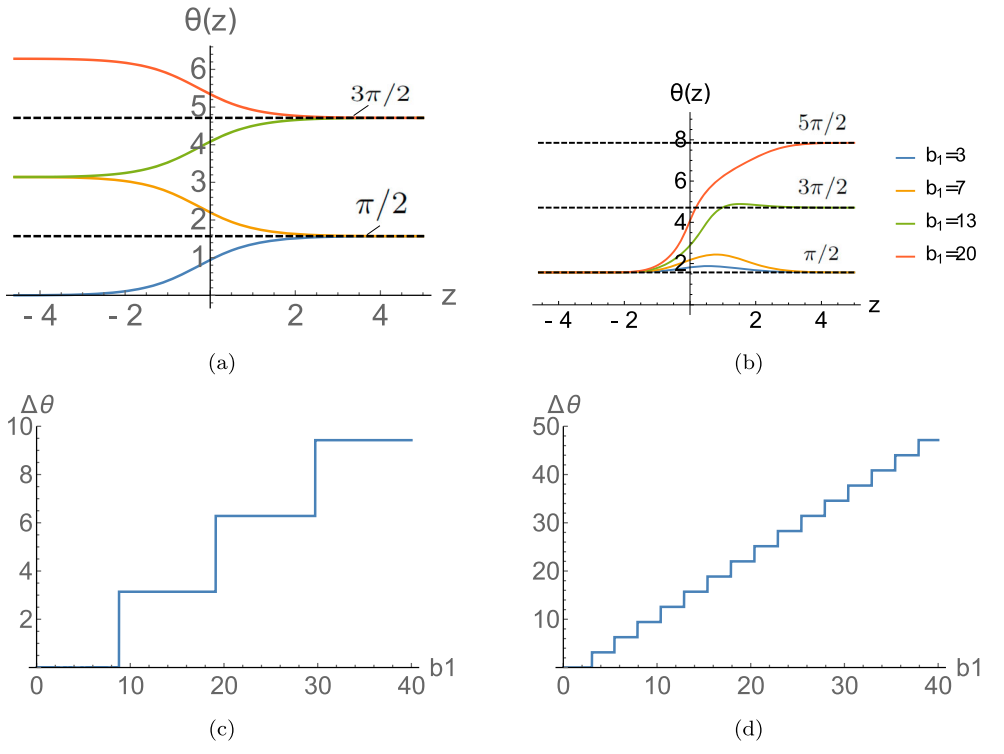

Figure 2. Example solutions of the linearised angle function (5) with $z_0 = -4.999 + 0.4$. Except where otherwise stated the parameters are $b_0 = 1$, $m = 0.5$, $l = 1$, $L = 1$, $z_0 = 5$ (the same as used in Wilmot-Smith and Hornig 2011). Panel (a), the case with no twist ($b_1 = 0$). Initial conditions are $\theta(z_i) = \pm 0.001, \pi \pm 0.001$, either side of the unstable equilibria $\theta = 0, \pi$. They tend towards the stable equilibra $\pi/2$ and $3\pi/2$, respectively. Panel (b), solutions with increased twisting with the initial condition $\pi/2$ (the fan plane of the $-z_0$ null), respectively, $b_1 = 3, 7, 13, 20$, as the twist is increased the solutions pass from tending to the $\pi/2$ to $3\pi/2$ and then $5\pi/2$. Panel (c) a plot of $\Delta\theta$ for increasing b_1 from an initial condition $\theta(z_i) = \pi/2$. Panel (d) the same plot as in (c) with $z_0 = 2.5$. (Colour online)

On increasing b_1 we pass through various critical values where the $\theta(z_i) = \pi/2$ field lines in the fan plane of the $-z_0$ null will tend towards $3\pi/2$ and then $5\pi/2$, as illustrated in figure 1(b). The dual equilibrium stability is what leads to this topological change in this model. If we consider the points initially in the $-z_0$ fan plane $\theta(z_i) = \pi/2$, and plot the net change in angle $\Delta\theta = \theta(z_0) - \pi/2$ as a function b_1, we obtain a discontinuous structure that jumps after the parameter b_1 passes critical values as shown in figure 1(c), these values depend on the various system parameters (cf. figure 1(c,d)). We shall see later that this jump coincides with the separator bifurcation detailed in (Wilmot-Smith and Hornig 2011).

The solutions shown in figure 2(a,b) use $\delta = 0.4$ for the initial conditions $\theta(z_i)$ with $z_i = -z_0 + \delta$, whilst the bifurcation plots use $\delta = 0.00001$, so that (essentially) the whole domain is accounted for. The choice of $\delta = 0.4$ was for visual convenience. When $\delta = 0.00001$ is used the $(z_0^2 - z^2)$ term in the equation's denominator ensures all solutions almost immediately tend towards $\theta = \pi/2, 3\pi/2$.

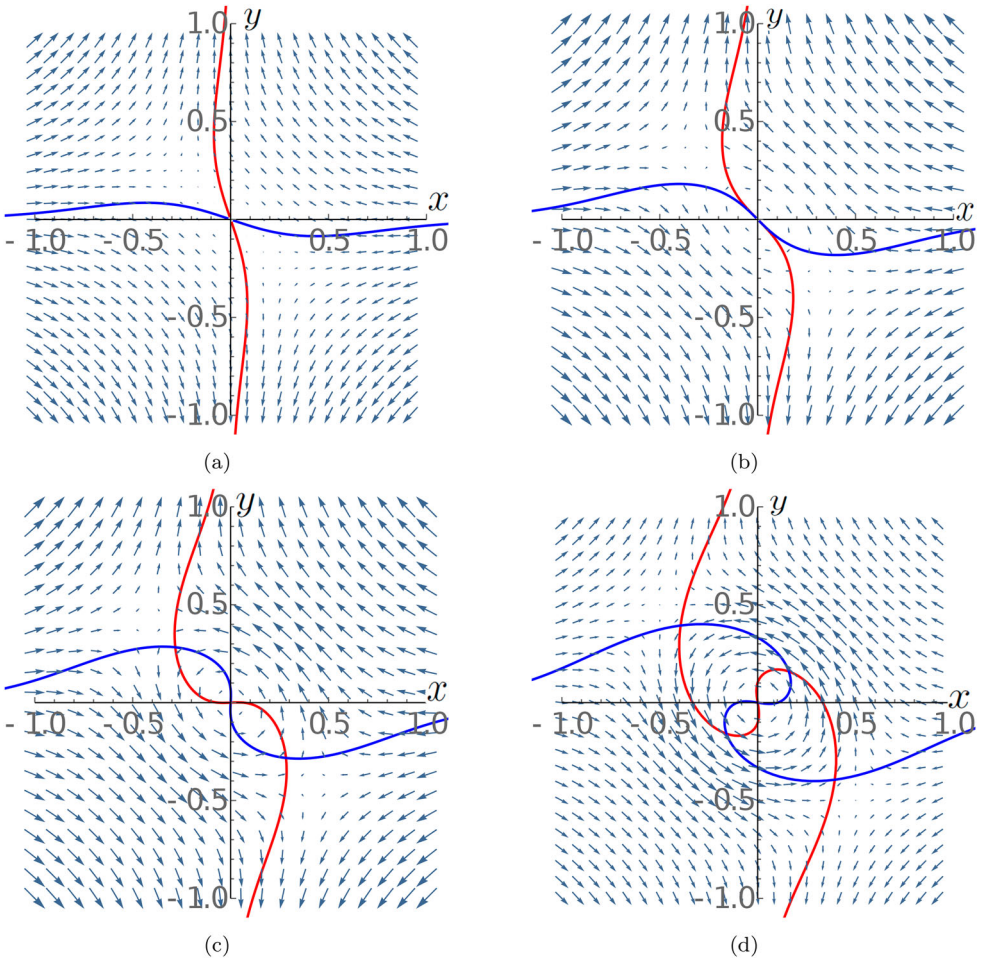

Figure 3. Plots of the map of the two fan planes from $-z_0 + \delta$ to $z = 0$ (red) and $z = z_0 - \delta$ to $z = 0$ (blue), for parameters $b_0 = 1, m = 0.5, l = 1, L = 1, z_0 = 5$ for $b_1 = 4, 8.796, 15, 25$. Slices of the vector field $\boldsymbol{B}_n + \boldsymbol{B}_t$ are shown for comparison to the figures in Wilmot-Smith and Hornig (2011). In panel (b) $b_1 = 8.796$ the two fan plane intersections are locally parallel at the separator $x = y = 0$. In panel (c) the separator bifurcation has occurred (note the two new intersections of the curves). In panel (d) a second bifurcation has occurred so there are now 5 separators. (Colour online)

2.2. *Fan plane maps, separator bifurcation and linking changes.*

As discussed in Wilmot-Smith and Hornig (2011), there is a bifurcation in the system as b_1 is increased, which becomes apparent when the two fan plane surfaces are mapped to $z = 0$ (from $-z_0$ and z_0), respectively. In such plots, the intersection of the two fan planes shows the position of the separators, this is illustrated in figure 3, the projection of the vector field $\boldsymbol{B}_n + \boldsymbol{B}_t$ is also superimposed. The exponential twist decay with radius from the separator causes the fan plane intersection curves to adopt sigmoidal shapes as b_1 is increased (panel (a)). We see at $b_1 = 8.796$, panel (b), this distortion causes the curves to be locally parallel in the neighbourhood of the origin. As b_1 is increased past this point, the separator bifurcation occurs as the curve's sigmoidal shape further develops leading to

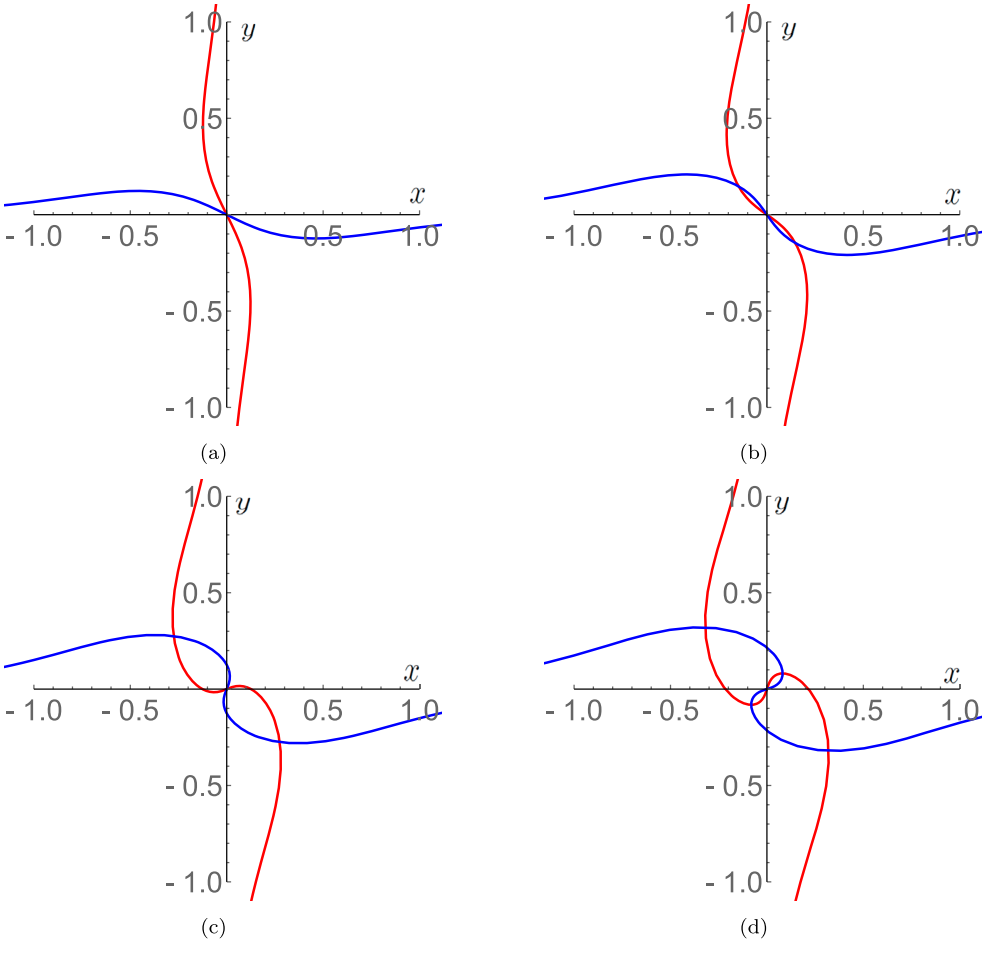

Figure 4. Plots of the map of the two fan planes from $-z_0 + \delta$ to $z = 0$ (red) and $z = z_0 - \delta$ to $z = 0$ (blue), for parameters $b_0 = 1$, $m = 0.5$, $I = 1$, $L = 1$, $z_0 = 2.5$ for $b_1 = 2, 3.5, 5, 6$. We see the first separator bifurcation between (a) and (b) then the second between (c) and (d). (Colour online)

two further intersections. By $b_1 = 25$ there has been one further bifurcation and there are now 5 separators. These plots recreate results found in Wilmot-Smith and Hornig (2011) where the parameter b_1 was modelled as $20t$, with $t = 0.41$ ($b_1 = 8.2$) given as when the first bifurcation occurred. Hereafter we omit the vector fields for clarity when we construct similar plots.

In fact we can make a more accurate estimate here as we note that $b_1 = 8.796$ is the value in figure 2(c) where the linearised system, a relatively simple uncoupled O.D.E registers a jump in the angle $\theta(z_0)$ when $\theta(z_i) = \pi/2$, which as we have seen means field lines from the fan plane of the $-z_0$ null *close to the original separator* reconnect from tending towards s^+ to s^-. The plot in figure 2(d) suggests that if we keep the same parameters but halve the value of z_0, we should see similar bifurcations between $b_1 = 2$ and 3.4, at $b_1 = 3.064$ and then 5 and 6, at $b_1 = 5.46$. This is confirmed in figure 4 and corresponds to a twist region spread over a relatively longer distance along the length of the separator.

The critical point from this analysis, which we will use to generalise, is that, because the twisting peaks at the separator, the linear approximation predicts the bifurcation.

2.2.1. Field line linking

A means of characterising the change in field topology, which has been noted in previous studies (e.g. Pontin and Wyper 2015) but not quantified as such, is the observation from the linear θ equation (5) that the separator bifurcation coincides with the reconnection and change in linking of the local fan plane curves. One can see this in figure 5. For a field with parameters $b_0 = 1$, $m = 0.5$, $l = 1$, $L = 1$, $z_0 = 5$, we have seen the first bifurcation occurs at $b_1 \approx 8.796$, in figure 5 we see plots of $\theta(z)$ with $\theta(z_i) = \pi/2$ and $\theta(z_i) = 3\pi/2$ for $b_1 = 8.7$, before the bifurcation and $b_1 = 8.9$ after it. We see the difference $\theta(z_0) - \theta(z_i)$ jumps from being zero in (a) to being π in (b). This also implies a jump in rotation in π of the two field lines, as illustrated in figure 5(c). The secondary bifurcation, which occurs for $b_1 = 19.116$, can be seen to induce an additional π winding of these field lines so that now they complete one full rotation with respect to each other. This winding is a well-known topological quantity $\mathcal{L}$ (Berger and Prior 2006), which in this case would be defined as

$$\mathcal{L} = \frac{\Delta\theta}{2\pi} + n. \tag{5}$$

Where n is a full integer number of turns of the fan plane around the separator. It is a topological invariant in that it is unchanged if the field lines deform without crossing while keeping their ends fixed. The sub-domains created by the intersection of the fan plane maps shown in figures 3 and 4 can then be seen to represent regions where the field lines intersecting the $z = 0$ surface which have distinct winding values with the separator. In effect, the system reconnects to develop a field with regions of inter-wound topology (as shown in Figure 5). The quantity $\mathcal{L}$ would be well defined even if the separator curve has a general geometry and this observation that the separator bifurcation coincides with jumps in $\mathcal{L}$ for subsets of the field will be utilised to deal with more general separator structures in sections 3 and 4.

2.3. Twisting as a predictor of the bifurcation

2.3.1. Twist

The linking L is related to a second quantity, the twist Tw (Berger and Prior 2006). This will be crucial in deriving practical bifurcation criteria in what follows, so we briefly sidetrack to define it clearly. The general definition applies to a ribbon structure. Consider a field line $\boldsymbol{x}$ and a unit vector field $\boldsymbol{V}$ which lies in the normal plane of $\boldsymbol{x}$, that is to say it is normal to the unit tangent curve of the axis: $\boldsymbol{T_x} = \mathrm{d}\boldsymbol{x}/\mathrm{d}s$. We can then define a second field line $\boldsymbol{y}$ through

$$\boldsymbol{y}(s) = \boldsymbol{x}(s) + \epsilon \boldsymbol{V}(s),$$

with ϵ the width of separation. The pair $(\boldsymbol{x}, \boldsymbol{y})$ form the ribbon structure. In solar physics, it could represent a flux rope localised on the curve $\boldsymbol{x}$. The twist represents the rotation of

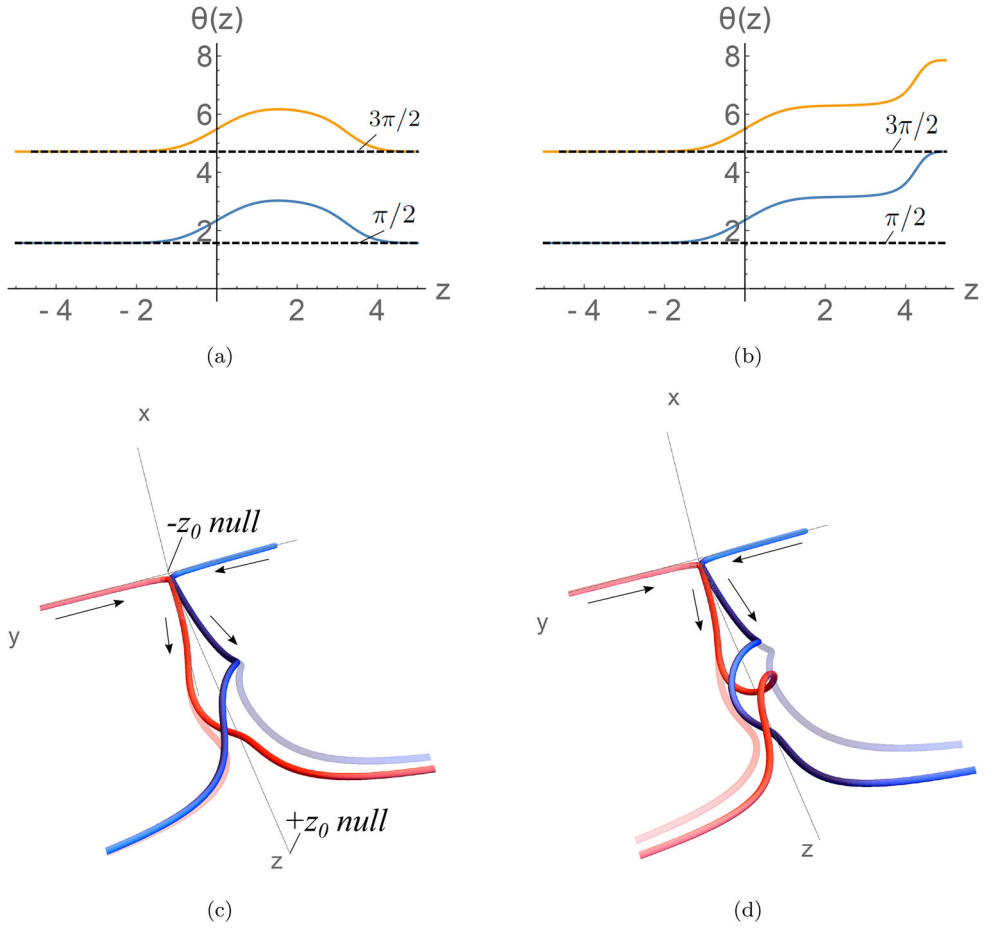

Figure 5. Depictions of the jump in net winding which accompanies the separator bifurcation process. Panel (a) shows solutions to (5) with $\theta(z_i) = \pi/2, 3\pi/2$ (points in the fan plane) with $b_1 = 8.7$, panel (b) for $b_1 = 8.9$. We see the change in angle for each solution jump from 0 to π. Panel (c) compares field lines for $b_1 = 8$ (opaque) and $b_1 = 9$ solid) which begin in the fan plane of the $-z_0$ null. The change in mutual angle is clear. Panel (d) compares field lines for $b_1 = 8$ (opaque) and $b_1 = 20$ solid) which begin in the fan plane of the $-z_0$ null. Here two of the bifurcations have occurred and now the end angles of the two curve sets are the same, but there is a clear twist in the core of the field for the $b_1 = 20$ curves. (Colour online)

the field $\boldsymbol{V}$ (the number of times which $\boldsymbol{y}$ rotates around $\boldsymbol{x}$)

$$Tw(\boldsymbol{x}, \boldsymbol{V}) = \frac{1}{2\pi} \int_{\boldsymbol{x}} \boldsymbol{T}_x(s) \cdot \boldsymbol{V}(s) \times \frac{\mathrm{d}\boldsymbol{V}(s)}{\mathrm{d}s} \, \mathrm{d}s. \tag{6}$$

In the case that the field line $\boldsymbol{x}$ is our separator $\boldsymbol{T} = (0, 0, 1)$ and the vector $\boldsymbol{V}$ given by $(\cos(\theta(z)), \sin(\theta(z)), 0)$ and one can see that

$$Tw = \frac{1}{2\pi} \int_{-z_0}^{z_0} \frac{\mathrm{d}\theta}{\mathrm{d}z} \mathrm{d}z = \mathcal{L}.$$

2.3.2. Mean twist

A second crucial quantity related to the twisting is the mean axial $\overline{Tw}$ twisting of a field line $\boldsymbol{x}$

$$\overline{Tw}(\boldsymbol{x}) = \frac{1}{2\pi}\int_{\boldsymbol{x}} \frac{\boldsymbol{B}\cdot\nabla\times\boldsymbol{B}}{\boldsymbol{B}\cdot\boldsymbol{B}}\,\mathrm{d}s, \tag{7}$$

where the curve is $\boldsymbol{x}$. This is the non-dimensionalised parallel current, for force free fields $\nabla\times\boldsymbol{B}=\alpha\boldsymbol{B}$ it is the parameter α and it is regularly calculated to characterise the developing topology of coronal force-free magnetic field extrapolations (e.g. Liu *et al.* 2016, Zhu and Wiegelmann 2019, Yang *et al.* 2020).

The similar notation to (6) indicates that (7) is, under certain circumstances, the average of (6) for all field lines forming the local flux surface surrounding the curve (Berger and Prior 2006, Liu *et al.* 2016). In particular, in the appendix of Liu *et al.* (2016), it is shown that the local asymmetric linear structure of the field determines the mean twist and the symmetric part the deviation of individual field line twist from the mean. We will see this clearly in our example. A critical caveat to this is that the effective comparison between the two quantities requires that the local field lines $\boldsymbol{y}$ remain in the neighbourhood of $\boldsymbol{x}$. This is generally a reasonable assumption for the fields considered in this study, except in the direct neighbourhood of the null where field lines diverge rapidly. For the case at hand this will not be a problem as there is no twist in the vicinity of the null, but it will become an issue in a later more general model.

2.4. Application to the case at hand

Using $\boldsymbol{B}=\boldsymbol{B}_c+\boldsymbol{B}_t$ and setting $\boldsymbol{x}$ to be the separator it can be checked that the mean twist is determined by $\boldsymbol{B}_t$

$$\overline{Tw}(\boldsymbol{x}) = \frac{1}{2\pi}\int_{\gamma} \frac{\boldsymbol{B_t}\cdot\nabla\times\boldsymbol{B_t}}{\boldsymbol{B_t}\cdot\boldsymbol{B_t}}\,\mathrm{d}s = \frac{1}{2\pi}\frac{(2b_1/m)\exp(-z^2/l^2)}{z_0^2-z^2}. \tag{8}$$

However the field line twisting/linking $\mathcal{L}$ around separator is

$$\mathcal{L} = Tw(\gamma) = \frac{1}{2\pi}\int_{-z_0}^{z_0}\frac{\mathrm{d}\theta}{\mathrm{d}z}\,\mathrm{d}z = \frac{1}{2\pi}\int_{-z_0}^{z_0}\frac{B_\theta(\gamma(z))}{rB_Z}\,\mathrm{d}z,$$

where the $\gamma(z)$ dependence of B_θ reflects the fact it depends on the θ value of the local field line wrapping around the separator. As discussed above this includes the nonlinear effect of the $\sin(2\theta)$ term. In this model, we can solve (4) for a given initial condition $\theta(z_i)$, with each $\theta_0=\theta(z_i)\in[0,2\pi)$ representing a field line, *i.e.* $Tw(\gamma)\equiv Tw(\theta_0)$. As one can see in figure 2(a), if $b_1=0$, then most field lines have a net twisting as they tend towards either $\pi/2$ or $3\pi/2$, due to the symmetric component of $\boldsymbol{B}_c$. But the symmetry of the system means there is as much positive as negative twisting and one can see that

$$\int_0^{2\pi} Tw(\theta_0)\,\mathrm{d}\theta_0 = \overline{Tw}(\gamma) = 0, \qquad \text{if} \quad b_1=0,$$

as the general theory predicts.

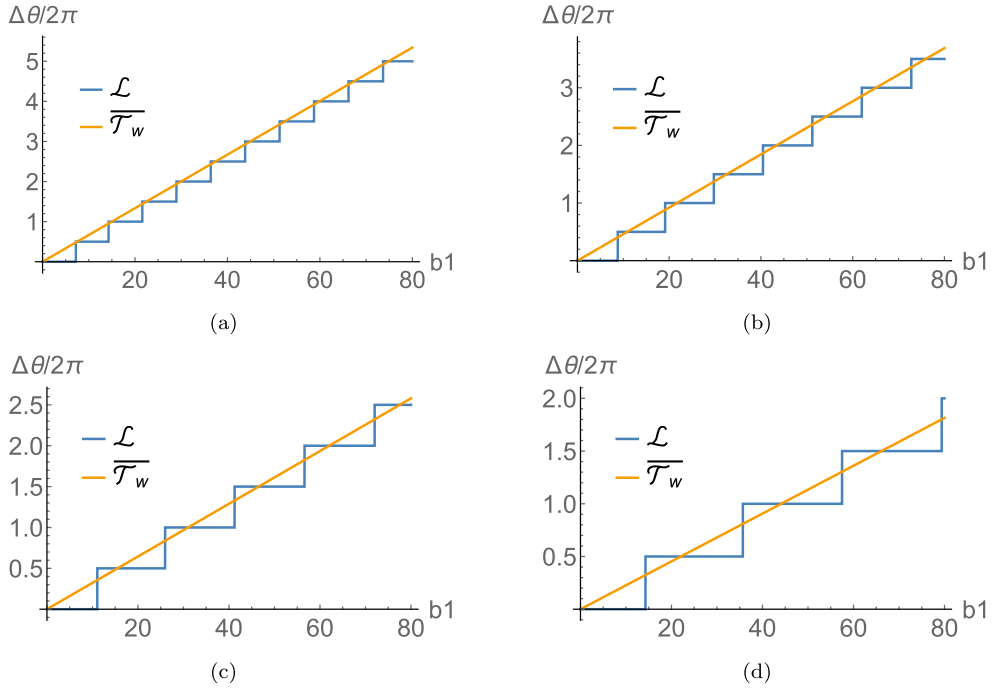

Figure 6. Comparisons of the variation in mean twisting $\overline{Tw}$. and the linking $\mathcal{L}$ of the fan plane curves with the separator, Parameters used are $b_0 = 1$, $m = 0.5$, $L = 1$, $z_0 = 5$ and $l = \sqrt{2}$ (a), $l = 1$ (b), $l = 1/\sqrt{2}$ (c) and $l = 1/\sqrt{4}$ (d). (Colour online)

2.5. Predictive criteria

2.5.1. Mean twist $\overline{Tw}$

If the mean twist $\overline{Tw}$ (8) could provide a good approximate prediction of the bifurcation it would be beneficial. In figure 6 we see the comparison of this quantity, evaluated as a function of b_1, overlaid on the critical value of $\mathcal{L} = T_w$ for the field line beginning at the $-z_0$ fan plane ($\theta_0 = \pi/2$), We vary the relative spatial extent of the twist distribution by using $b_0 = 1, m = 0.5, L = 1, z_0 = 5$ and various values of the parameter l which controls the exponential decay of $\boldsymbol{B}_t$ about $z = 0$. For $l = \sqrt{2}$ the twist is significant for most the domain, while at the other end with $l = 1/\sqrt{4}$ is only significant on $\approx z \in [-1.7, 1.7]$. We see the estimate is very good when the twist is spread out on the whole domain, but less so when the twist is highly localised. Even in the case of $l = 1/\sqrt{4}$ it is consistently true that when $\overline{Tw}$ reaches a multiple of 0.5 then $\mathcal{L}$ will have that value. Therefore, $\overline{Tw}$ could potentially provide a threshold for bifurcation but is generally an underestimate.

To further test the strength of $\overline{Tw}$ and Tw as predictors, in figure 7(a), we see various solutions to the equation

$$\frac{\mathrm{d}\theta}{\mathrm{d}z} = \frac{3z_0 \sin(2\theta) + (2b_1/m)(\sin(3\pi z) + \frac{1}{2}) \exp(-z^2/l^2)}{z_0^2 - z^2}, \tag{9}$$

which includes a sinusoidal variation in the current along the separator's length. We see this sinusoid manifest in the variation in angle. In panel (b) we see the plot of the change in

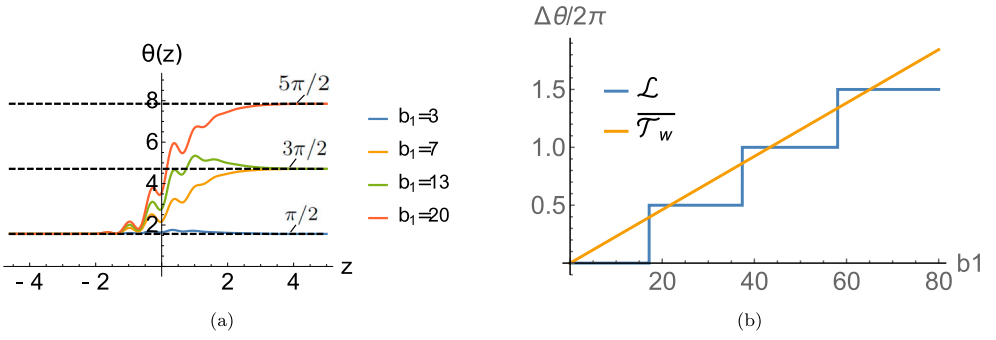

Figure 7. Plots the fan plane twisting bifurcation (local to the separator) of a sinusoidally varying current. Panel (a), solutions to (9) for $b_0 = 1$, $m = 0.5$, $L = 1$, $z_0 = 5$ for various b_1 values. Panel (b), comparisons of the variation in mean twisting $\overline{Tw}$ and the linking $\mathcal{L}$ of the fan plane curves with the separator in this sinusoidally varying twist model. (Colour online)

linking with b_1 ($\Delta\mathcal{L}$) from the initial value (zero here). Also shown is the increase in mean twist with b_1, we see a similar quality of prediction to the purely exponential case (Panel (b) of figure 6 has the same parameters).

2.5.2. The maximum linkage $\mathcal{L}^M$

We observe that the first bifurcation occurs when the angle θ, initially $\pi/2$, reaches, π (figure 5(b)). After this the $\sin(2\theta)$ term of (2) will ensure the angle tends to $3\pi/2$. As shown in figure 5(a), if it just fails to reach π, the $\sin(2\theta)$ eventually sends it back to $\pi/2$. If we define the linking as a function of the integration domain $z \in (-z_0, z]$:

$$\mathcal{L}(z) = \frac{1}{2\pi}\int_{-z_0}^{z} \frac{\mathrm{d}\theta}{\mathrm{d}z}\,\mathrm{d}z, \tag{10}$$

then the angle change $\pi/2$ to π represents a linking $\mathcal{L}(z)$ of 0.25 for some $z \in [-z_0, z_0]$, So the critical criteria is that the maximum value of $\mathcal{L}(z)$ reaches a multiple of 0.25, We define this quantity $\mathcal{L}^M$ as:

$$\mathcal{L}^M = \max_{z\in[-z_0,z_0]} \mathcal{L}(z),$$

where $\mathcal{L}(z)$ is given by (10).

We see in figure 8 that $\mathcal{L}^M$ has exactly the predictive properties we require as $\mathcal{L}^M$ tends continuously to a multiple of 0.25 just before bifurcation, for each bifurcation. Thus one could have predicted how close the system was to bifurcation in advance, One caveat to this observation is that it is possible for a current model which reverses sign to obtain a value of $\mathcal{L}^M$ above 0.25 then, if the twisting caused by this current is reversed, the angle θ, drops back below π before reaching $z = z_0$ and the null structure at $z = z_0$ will then ensure it tends to $\pi/2$, so the bifurcation does not occur. An explicit example of this is a linearised system in the form

$$\frac{\mathrm{d}\theta}{\mathrm{d}z} = \frac{3z_0\sin(2\theta) - (2b_1 z/(ml^2))\exp(-z^2/l^2)\cos((z+5)/8)}{z_0^2 - z^2}, \tag{11}$$

whose axial twist reverses sign around $z = 0$, but which reaches a higher peak rate when $z < 0$ owing to the cos function. This imbalance means it eventually bifurcates for a high

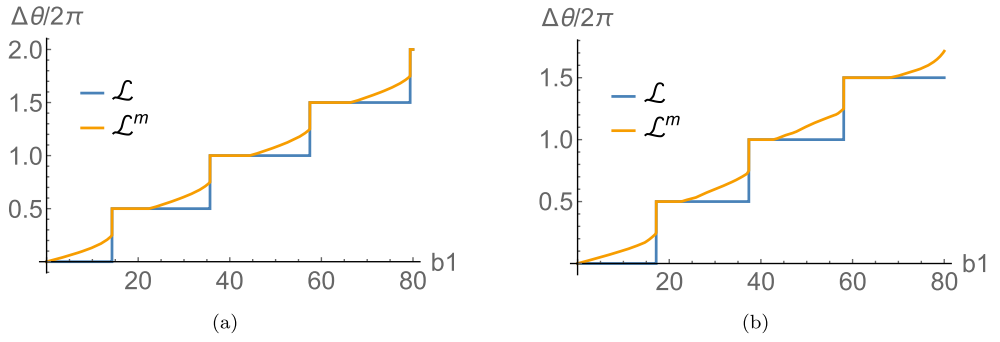

Figure 8. Demonstrations that the maximum achieved linking L^m can be used as a bifurcation criteria. Panel (a) a comparison of $\mathcal{L}^M$ and $\mathcal{L}$ for $l = 1/\sqrt{2}$, the case shown in figure 6(d). Panel (b), the same plot for the sinusoidally varying twist whose bifurcation staircase is shown in figure 7. (Colour online)

enough b_1 value but the maximum linking $\mathcal{L}^m$ increases much more quickly, as shown in figure 9(a). In fact this model highlights a second interesting possibility, which we might call temporary or intermittent bifurcation. At about $b_1 \approx 62$, we see in figure 9(a) that there is a bifurcation which then persists until $b_1 \approx 69$ when the bifurcation is reversed. Then at $b_1 \approx 78$ a more permanent bifurcation occurs. We see in figure 9(b) example solutions indicating what causes the intermittent bifurcation. All solutions (for various b_1) show the expected rise then decay of θ due to twist reversal. As b_1 is increased, the peak value of θ increases as expected. Comparing the solutions during the intermittent bifurcation $b_1 = 63$ and just after it $b_1 = 72$, we see that the sharper decay phase for $z > 0$ in the $b_1 = 72$ solution pushes it back below π where it does not for $b_1 = 63$. This occurs because the $\sin(2\theta)$ function, which is negative when $n\pi/2 < \theta < (n+1)\pi/2$, $n = 1, 3, 5\ldots$, tends to boost the decay of θ when θ takes values in these ranges. In the $b_1 = 72$ case the maximum decay rate (just after $z = 0$) is reached when $\sin(2\theta)$ is negative (approx $\theta = 11.5$), so it is boosted at its peak rate of decay. This is by contrast to the $b_1 = 63$ case, which peaks at a value when $\sin(2\theta)$ is positive (approx $\theta = 10.5$) so that its maximum decay rate is reduced. Eventually a sufficient b_1 value ensures the maximal peak of θ is too large to overcome, thus causing the permanent bifurcation.

We should stress this is a contrived example to demonstrate a mathematical property of separator bifurcation rather than one we might expect to see in reality. Developing a mixed bifurcation diagnostic in this case, however, should yield a robust bifurcation prediction criterion.

We can additionally incorporate the information in the mean twisting $\overline{Tw}$. We see in figure 9(c) that when $\mathcal{L}^M$ works as a bifurcation prediction criteria for monotonic twisting/current, the twist is always greater than $\mathcal{L}^M$ prior to bifurcation. For the twist/current reversal model, the mean twist $\overline{Tw}$ captures the rotational reversal. In figure 9(d) we see plots of $\mathcal{L}$, $\mathcal{L}^m \mod 0.25$ and $\overline{Tw}$ for the reversal model (11). The quantity $\mathcal{L}^m \mod 0.25$ reaches numerous peaks where $\overline{Tw}$ is significantly below its value, indicating they are false predictive signals. We see the intermittent bifurcation is not found when $\mathcal{L}^m$ is 0.25, but we note the twist value gets very close to 0.25 at its onset. By contrast, the permanent bifurcation is reached when $\mathcal{L}^m$ reaches a multiple of 0.25, which is also the first bifurcation where the mean twist is above 0.25. After this, there are a number of points at which $\mathcal{L}^m$ reaches a multiple of 0.25 but which do not indicate a bifurcation. Again the value of $\overline{Tw}$

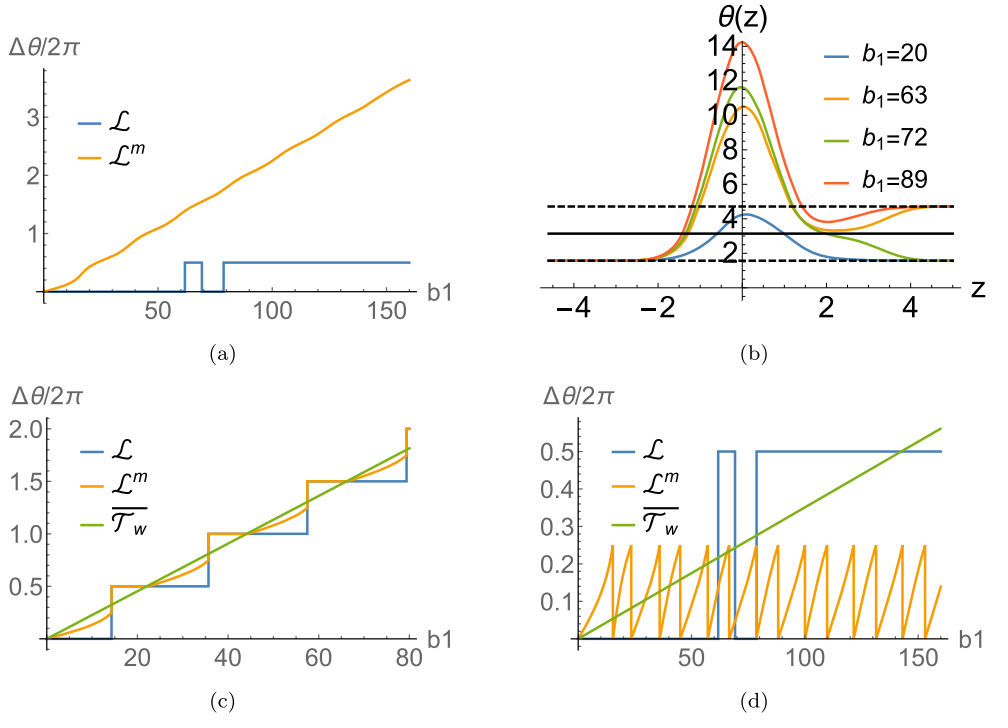

Figure 9. Using $\mathcal{L}^m$ and $\overline{Tw}$ to predict permanent bifurcations. Panel (a) plots pf $\mathcal{L}$ and $\mathcal{L}^m$ for the sign reversal twist system (11). $\mathcal{L}$ shows a temporary bifurcation at $b_1 \approx 62$, then a more permanent bifurcation at $b_1 \approx 79$ Panel (b) example solutions for $\theta(s)$ to 11) for various b_1 before ($b_1 = 20$) during ($b_1 = 63$) and after ($b_1 = 72$) the intermittent bifurcation, and after the permanent bifurcation $b_1 = 89$. The dashed horizontal lines are $\pi/2$ and $3\pi/2$, the solid one $\theta = \pi$. Panel (c) a comparison of $\overline{Tw}$ and $\mathcal{L}^m$ for the case shown in figure 8(b), we see $\overline{Tw}$ is consistently above $\mathcal{L}^m$ at bifurcation. Panel (d) a comparison of $\mathcal{L}$, $\mathcal{L}^m \mod 0.25$ and $\overline{Tw}$ for the same solutions as panel (a). We, see, as discussed in the text, $\overline{Tw}$ give an indication of when the bifurcation is likely to be permanent. (Colour online)

is providing a corrective here. The next bifurcation would require $\overline{Tw}$ just above 0.75 and this has not been attained for any of the peaks in the quantity $\mathcal{L}^m \mod 0.25$.

So we conclude this section by proposing that the following procedure can be used to infer if a separator is close to bifurcation in our model, when an increasing current is developed along the separator (increasing in terms of its extremal value):

- Calculate $\mathcal{L}^M$. If $\mathcal{L}^M \mod 0.25$ is close to 0.25, then we consider the separator might be close to bifurcation.
- If further $\overline{Tw} > n - 1 + 0.25$ when $\mathcal{L}^M \mod 0.25$ is close to 0.25, for the nth potential bifurcation, then we conclude that the separator is indeed close to a permanent bifurcation.
- If $\overline{Tw}$ gets close to $n-1+0.25$, but $\mathcal{L}^M \mod 0.25$ is not too close to 0.25, we consider that any separator bifurcation located might be intermittent or temporary.

We also note that if the axial current $\boldsymbol{B} \cdot \nabla \times \boldsymbol{B}$ is of one sign (chirality), then calculating $\mathcal{L}^M$ alone should be sufficient.

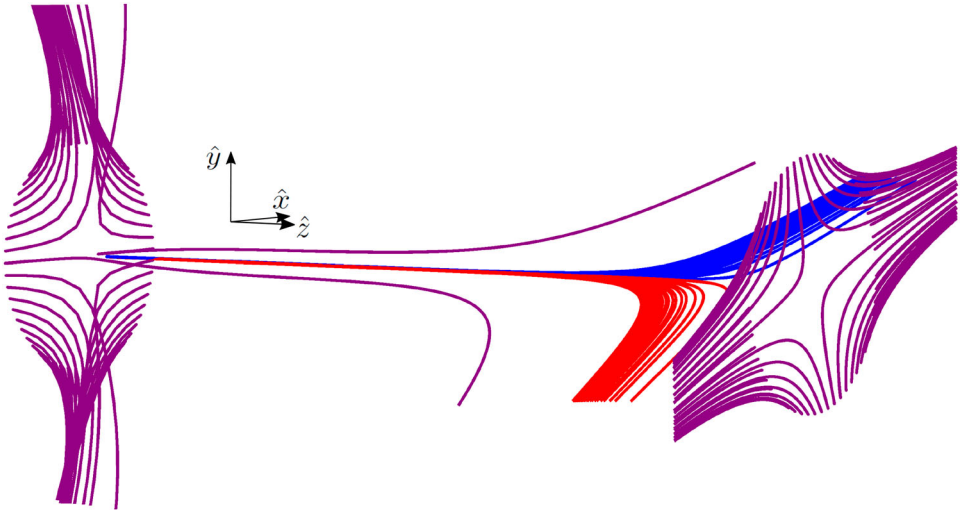

Figure 10. An example of the general null structure $\boldsymbol{B}_g$ (12b), with $b_0 = L = 1$ and $a = 0.5$, $b = 1.2$, $c = 3$. (Colour online)

3. A more general separator model

To test these criteria further, we now consider the following generalised null-separator model introduced in (Stevenson *et al.* 2015) which is described by three scalar parameters a, b, c

$$\boldsymbol{B}_g = B_{gx}\hat{\boldsymbol{x}} + B_{gy}\hat{\boldsymbol{y}} + B_{gz}\hat{\boldsymbol{z}}, \tag{12a}$$

$$B_{gx} = \frac{b_0}{L^2}[-4axz_0 + by(z+z_0) + cx(z+z_0)], \tag{12b}$$

$$B_{gy} = \frac{b_0}{L^2}[y(2a-c)(z+z_0) + 2ayz_0 + bx(z+z_0)], \tag{12c}$$

$$B_{gz} = \frac{b_0}{L^2}y^2\left[\left(a - \frac{1}{2}c\right) + a(2z_0(z+z_0) - (z+z_0)^2) + bxy + \frac{1}{2}cx^2\right]. \tag{12d}$$

The expression here is scaled from that given in Stevenson *et al.* (2015), from $[0, L]$ to $[-z_0, z_0]$, and corrects a typo on the first term of B_{gx} in that text. Varying the parameters a and c modifies the geometry of the field lines in the separatrix surfaces of both nulls. There are some conditions on their values (see Stevenson *et al.* 2015). Varying the parameter b rotates the z_0 null's separatrix surface relative to the lower null's separatrix surface. The case considered in the previous section corresponds to the parameter set $a = c = 1$, $b = 0$. So that the default, $b = 0$, has the fan plane of one null aligned with the spine of the other null. Altering b then breaks this alignment, as shown in figure 10, which, as we shall see shortly, imparts a built in rotation to the system into the field lines in the local neighbourhood of the separator even in the absence of a localised twist region.

The cylindrical version of the field $\boldsymbol{B}_g + \boldsymbol{B}_t$ is

$$\frac{\mathrm{d}\theta}{\mathrm{d}z} = \frac{2\{F + 2b_1[L^2/(at)]\exp(-r^2/(at) - z^2/l^2)\}}{b_0\{r^2[(c-a)\cos(2\theta) + b\sin(2\theta)] + a(r^2 - 2z^2 + 2z_0^2)\}}, \tag{13a}$$

$$\frac{\mathrm{d}r}{\mathrm{d}z} = \frac{2r\{\cos(2\theta)[c(z+z_0) - a(z+4z_0)] + az + b\sin(2\theta)(z+z_0)\}}{r^2[(c-a)\cos(2\theta) + b\sin(2\theta)] + a(r^2 - 2z^2 + 2z_0^2)}, \tag{13b}$$

where

$$F = b_0\{\sin(2\theta)[a(z+4z_0) - c(z+z_0)] + b\cos(2\theta)(z+z_0)\}.$$

As with the previous case, the equation obtained by expanding in r around the separator ($r = 0$) leads to a de-coupled angle equation

$$\frac{\mathrm{d}\theta}{\mathrm{d}z} = \frac{F + 2b_1[L^2/(at)]\exp(-z^2/l^2)}{ab_0(z_0^2 - z^2)}. \tag{14}$$

3.1. A built in rotation

As in the previous section, we first consider the twist-free case $b_1 = 0$. As with (4) the denominator tends to zero at the null points $\pm z_0$, but, unlike that case there is an explicit z dependence in the numerator. This z dependence arises from the fact that the fan plane of the $-z_0$ null no longer aligns with the spine direction of the z_0 null. This leads to a rotation of the field lines connecting the (local) fan plane of the z_0 null to the spine directions s^- (or s^+), as can be observed in figure 10. This angle can be characterised as follows. At $z = -z_0$ the numerator is

$$a3b_0z_0\sin(2\theta).$$

So the spine directions of the $-z_0$ null are represented by $\theta = 0, \pi$ and the fan plane $\pi/2, 3\pi/2$ as in the initial case. For general $z > 0$ the four zeros of the numerator (when taken mod 2π) are

$$\tfrac{1}{2}\arctan(A/B) + n\pi/2, \qquad (n = 0, 1, 2, 3), \tag{15a}$$

where

$$A = c(z+z_0) - a(z+4z_0), \qquad B = -b(z+z_0). \tag{15b}$$

The development of these zeros for $z \in [-z_0, z_0]$ are shown in figure 11(a) as dashed lines. Also shown in this same figure are solutions to (14) beginning at $\theta = 0, \pi/2, \pi, 3\pi/2$. The field lines starting at $0, \pi/2$ tend towards $\frac{1}{2}\arctan A(z_0)/B(z_0) + \pi/2$, i.e. the field lines tend to s^+, and those starting at $3\pi/2, \pi$ and $3\pi/2$ tend to $\frac{1}{2}\arctan(A(z_0)/B(z_0)) + 3\pi/2$ (tending to s^-). This leads to a natural inbuilt rotation, or linking $\mathcal{L}_0(z) =$

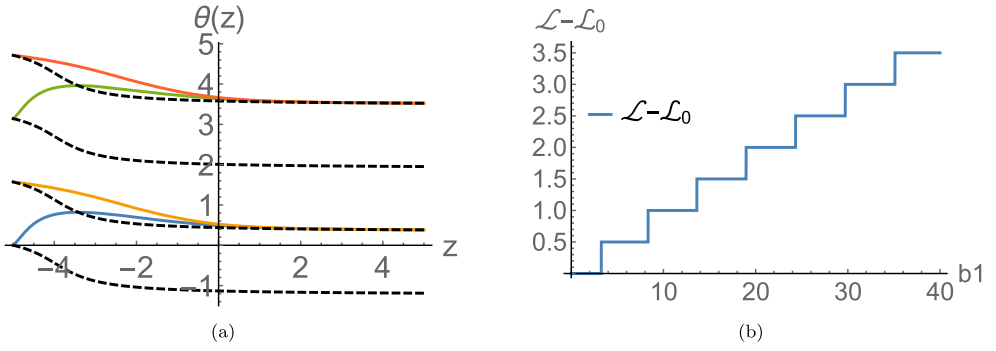

Figure 11. Solutions of (14). Panel (a) solutions as a function of z for $b_0 = 1$, $m = 0.5$, $l = 1$, $L = 1$, $z_0 = 5$, $a = 0.5$, $b = 1.2$, $c = 2$ and initial conditions beginning at the fan planes and spine direction of the $-z_0$ null. The dashed lines are the angles (15a) which are the zero values of the numerator (14). Panel (b) the value of $\Delta\theta$ for increasing b_1 for the same parameters as in (a). (Colour online)

$\frac{1}{2}\pi^{-1}\arctan(A(z)/B(z))$. Thus it is the quantity

$$\Delta L = \mathcal{L}(z_0) - \mathcal{L}_0(z_0),$$

which must be tracked to locate bifurcations. We also modify the critical linking to take the following value

$$\mathcal{L}^M = \max_{z\in[-z_0,z_0]} \mathcal{L}(z) - \mathcal{L}_0(z).$$

As one would expect, there is a similar bifurcation structure to the system as studied in the previous section. That is to say there is a series of jumps in end angle of π for increasing applied twist b_1, or jumps in $\mathcal{L} - \mathcal{L}_0$ of $\frac{1}{2}$, as shown in figure 11(b). We confirm in figure 12(a–d) that the jumps shown in figure 11(b) correspond to the same bifurcation structure as in the previous section, that is the maps of the null fan surfaces at z_0 pass through several configurations where they are locally tangential at the initial separator, thus generating regions of distinct topological linkage at the field's interior.

Finally, as shown in figure 13 that the combination of $\overline{Tw}$ and $\mathcal{L}^M$ can be used to predict when the system is close to bifurcation as in last section (when $\mathcal{L}_0(z) = 0$ for all z).

4. General separator geometry

The winding $\mathcal{L}$ can be defined for pairs of curves with arbitrary geometry (Berger and Prior 2006), so we can extend the bifurcation criteria to cases for which the separator is not a straight line. To do so we first define a field with a separator which is curved. We use an offset twist

$$\boldsymbol{B}_{to} = \frac{2b_1}{m}\exp\left(-\frac{(x-x_0)^2+(y-y_0)^2}{m^2} - \frac{z^2}{l^2}\right)[-y\hat{\boldsymbol{x}} + x\hat{\boldsymbol{y}}], \tag{16}$$

with (x_0, y_0) the location of the twisting core, away from the separator. The action of this twist is to distort the initially straight ($b_1 = 0$) separator. Then we consider the field $\boldsymbol{B}_n + \boldsymbol{B}_{to}$ with $\boldsymbol{B}_n$ given by (1). As b_1 is increased the two fan planes distort and their intersection takes on a distorted geometry (figure 14(a)). Here we use the parameters $b_0 = 1$,

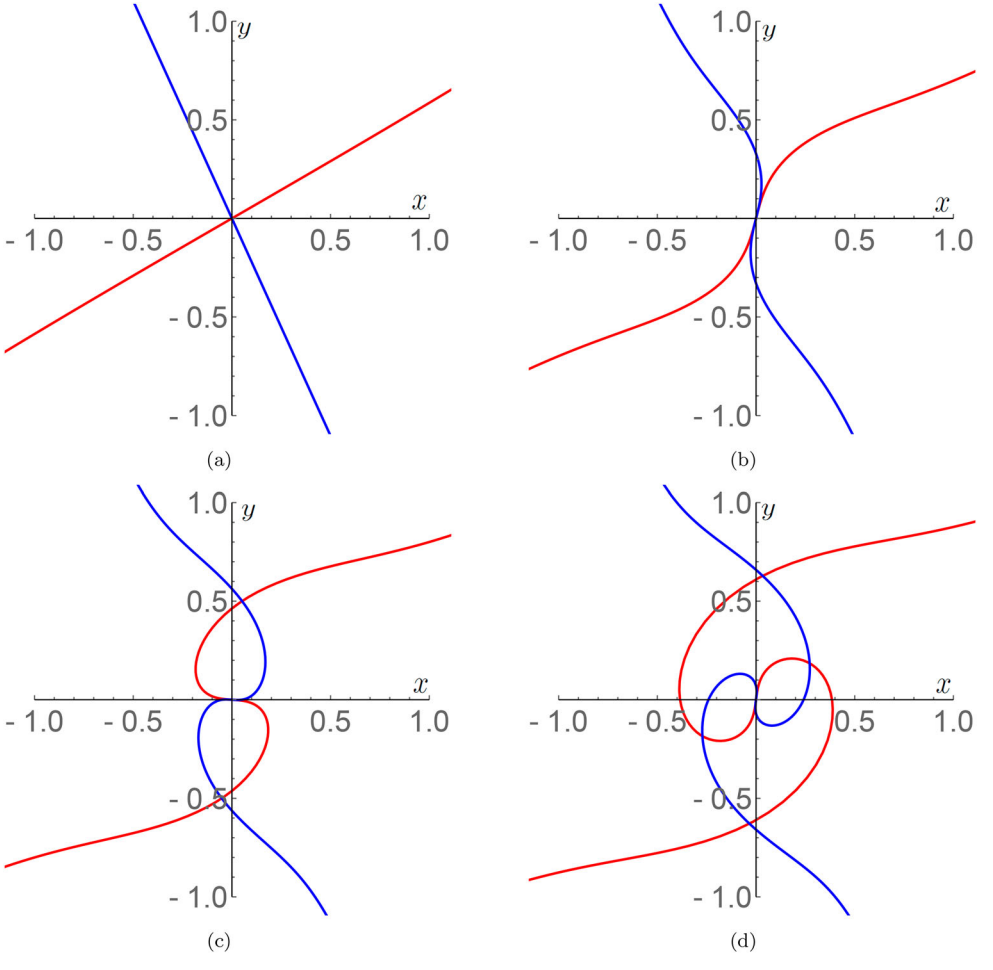

Figure 12. Separator bifurcations for the system defined by equations (13a) for $b_0 = 1, m = 0.5, l = 1, L = 1, z_0 = 5, a = 0.5, b = 1.2, c = 2$. The parameters used to generate these plots as the same used to generate the $\mathcal{L}$ plot shown in figure 11(b). The twist parameters for each panel are (a) $b_1 = 0$, (b) $b_1 = 4.06$, (c) $b_1 = 9.08$ and (d) $b_1 = 14.31$. (Colour online)

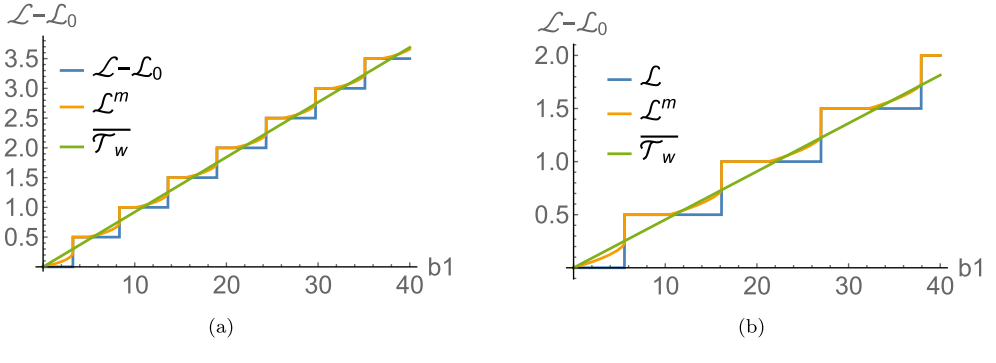

Figure 13. Comparisons of the quantity $\Delta\theta$ for b_1 for solutions to 14 and the mean twist $\overline{Tw}$. Panel (a), parameters $b_0 = 1, m = 0.5, l = 1, L = 1, z_0 = 5, a = 0.5, b = 1.2, c = 2$. Panel (b), parameters $b_0 = 1, m = 0.5, l = 0.5, L = 1, z_0 = 5, a = 0.5, b = 1.2, c = 2$. (Colour online)

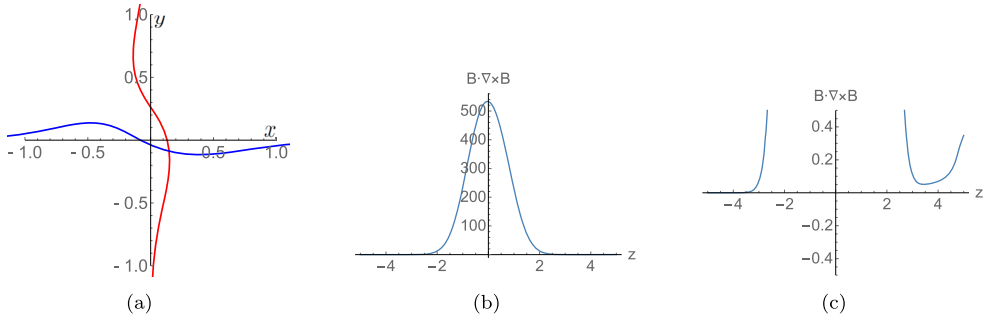

Figure 14. Properties of the distorted separator model. Panel (a) is the fan plane maps to $z = 0$ of the initial field $\boldsymbol{B}_n + \boldsymbol{B}_{to}$. The separator's distortion is clear by its off-axis location. Panel (b), the local axial "current" $\boldsymbol{B} \cdot \nabla \times \boldsymbol{B}$ for the field. Panel (c) the plot in (b) shown with a smaller range to emphasise there is a non-zero separator current in the neighbourhood of the second null at z_0. (Colour online)

$m = 0.5$, $l = 1$, $L = 1$, $z_0 = 5$, $x_0 = 0$, $y_0 = 0.2$ and $b_1 = 7$ to create the fan plane intersection geometry shown in figure 14(a). This separator curve will be labelled as $\boldsymbol{x}(s) = (x_s(z), y_s(z), z)$ and the applied current centred on this field line will take the following form:

$$\boldsymbol{B}_s = t\ \exp(-10((x - x_s)^2 + (y - y_s)^2) - \tfrac{1}{2}z^2)[-(y - y_s)\hat{\boldsymbol{x}} + (x - x_s)\hat{\boldsymbol{y}}], \tag{17}$$

where the parameter t will control the strength of the applied current. In this case, for variation, we apply a negative current, $t < 0$. The field then takes the form $\boldsymbol{B}_n + \boldsymbol{B}_s + \boldsymbol{B}_{to}$. It should be pointed out this is not aimed at modelling a specific phenomenon and is simply derived to demonstrate the flexibility of the bifurcation criteria developed here. There are a couple of reasons for this choice of field in particular. First, it is not a purely axial current unlike the previous cases. The magnitude of the field $\boldsymbol{B}_s$ peaks along the separator curve $\boldsymbol{x}_s$, but its axial component $\boldsymbol{B} \cdot \mathrm{d}\boldsymbol{x}_s/\mathrm{d}s$ varies along the length of the separator, as shown in figure 14(b). This, along with the separator geometry ensures there is a non-constant current along the separator, including in the locality of the z_0 null (figure 14(c)), a more general scenario than previously considered. Second, since we do not have an analytical form of the curve $\boldsymbol{x}_s$, we have to use standard field line tracing techniques to calculate the quantity $\mathcal{L}$. This is by contrast to the cases above where we had clear nonlinear o.d.e for the linear behaviour of the angle θ, which would not in general be available.

The procedure for identifying separator bifurcations is as follows:

- Identify the separator field line $\boldsymbol{x}_s$ by mapping out the two fan surfaces (we used bisection to identify the start coordinates of the separator (x_{s0}, y_{s0}, z_0)).
- Using an initial condition $(x_{s0}, y_{s0}, z_0) + \boldsymbol{\delta}$ with $\boldsymbol{\delta}$ a small vector which points along the fan plane of the chosen "launch null" (here we use $|\delta| = 1 \times 10^{-8}$). Using this initial condition trace out a second curve $\boldsymbol{x}_{s\delta}(t)$ which represents the local behaviour of the fan plane map in the neighbourhood $\boldsymbol{x}_s$ (this will change as t varies).
- Calculate the winding $\mathcal{L}(\boldsymbol{x}_s, \boldsymbol{x}_{s\delta}(t))$ of the two curves, this estimates the behaviour of the function $\theta(s)$. The precise formula calculating $\mathcal{L}$ in the general case was derived in Berger and Prior (2006) and is described in the appendix.

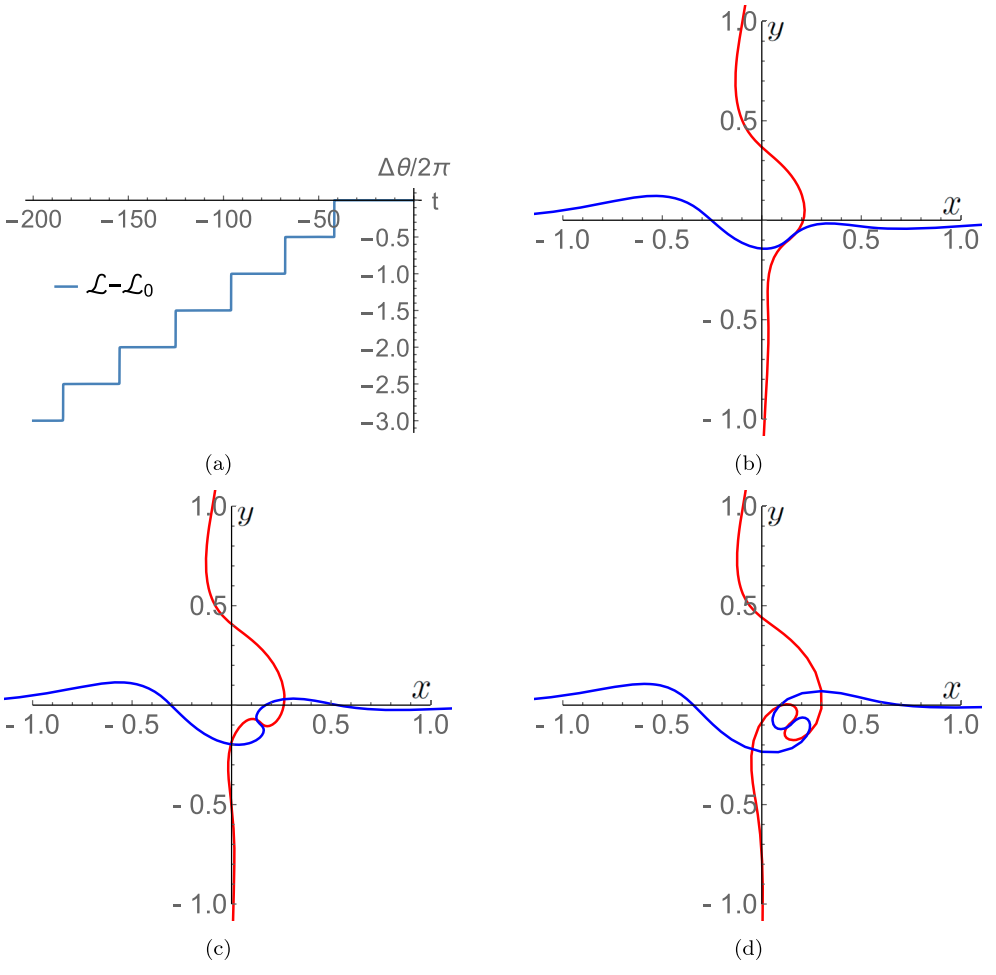

Figure 15. Bifurcation figures for the field $\boldsymbol{B}_n + \boldsymbol{B}_s + \boldsymbol{B}_t$. Panel (a), the bifurcation staircase diagram as a function of the twisting parameter t of (17). Panel (b), the first bifurcation at $t = -41.7604$. Panel (b), the second bifurcation at $t = -67.599$. Panel (c), the third bifurcation at $t = -95.974$. (Colour online)

- Repeat this procedure for steadily increased t (or increasing magnitude of the applied current in the system modelled). When jumps of magnitude 0.5 in $\mathcal{L}$ are obtained one has identified a bifurcation.

We see the results of this procedure in figure 15(a). The initial bifurcation requires a larger change in value than the subsequent bifurcations as the local twisting structure is significantly irregular. The increase (in magnitude) of the parameter t allows twisting along the axis of the curve to become dominant. After the first bifurcation, the bifurcations occur at regular intervals with a gradual decrease in the parameter t. The first three bifurcations are pictured in panels (b)–(d).

We applied this method of bifurcation analysis to all the previous fields and found it recreated all the bifurcation staircase diagrams precisely. The aim now is to see

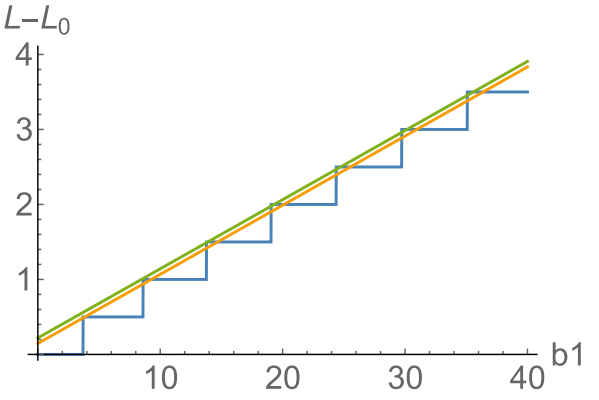

Figure 16. A comparison of Linking/separator bifurcation plots for (21) and plots of $\overline{Tw}$ on the reduced domain, given by (23) with $C = 1, 10$. (Colour online)

generalisations of the bifurcation prediction quantities $\overline{Tw}$ and $\mathcal{L}^m$ can be used to predict how close the system is to separator bifurcation.

4.1. Extending the predictive criteria

4.1.1. Extension of $\mathcal{L}^m$

The definition of $\mathcal{L}^m$ given in the previous section

$$\mathcal{L}^M = \max_{z\in[-z_0,z_0]} \mathcal{L}(z) - \mathcal{L}_0(z),$$

needs only minor modifications. We can define subsections of the field lines $\boldsymbol{x}_s$ and $\boldsymbol{x}_{s\delta}(t)$ on $[0, l] \subset [0, L]$, where L is the arclength of the field line $\boldsymbol{x}_s$. We label these subsets as $\boldsymbol{x}_s^l$ and $\boldsymbol{x}_{s\delta}^l(t)$. One could use z rather than l if the field lines are monotonic in z, but an arclength parameterisation l allows for more general curves. We define

$$\mathcal{L}(l) = \mathcal{L}(\boldsymbol{x}_s^l, \boldsymbol{x}_{s\delta}^l(t)), \qquad \mathcal{L}_0(l) = \mathcal{L}(\boldsymbol{x}_s^l, \boldsymbol{x}_{s\delta}^l(0)), \tag{18}$$

and

$$\mathcal{L}^M = \max_{l\in[0,L]} \mathcal{L}(l) - \mathcal{L}_0(l). \tag{19}$$

Note that the definition of $\mathcal{L}^M$ is parameterisation independent, arclength parameterisation is simply a convenient one. We see in figure 17(a) this measure works almost exactly as it did in the previous sections, rising to multiples of 0.25 continuously just before bifurcation. For the first bifurcation, $\mathcal{L}^M = 0.25$, the rise to 0.25 is relatively sharp, indicating that the precise notion of "close" to bifurcation should not only take into account the value of $\mathcal{L}^M$, but its rate of increase.

4.1.2. Mean twist $\overline{Tw}$ and avoiding its divergence

The idea is to calculate the quantity

$$\overline{Tw}(\boldsymbol{x}_s).$$

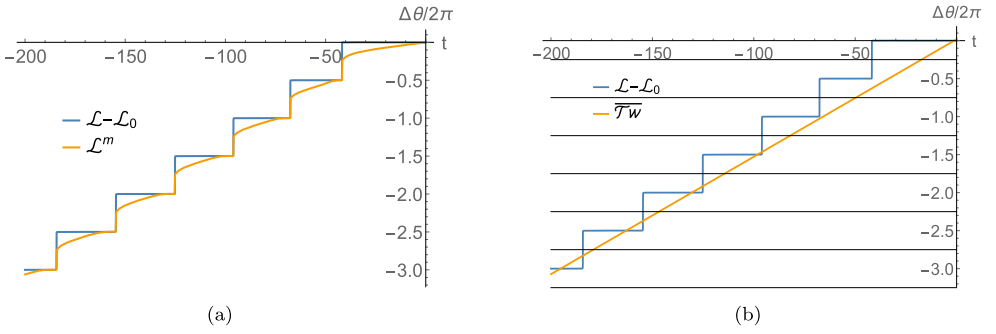

Figure 17. Applications of the predictive separator bifurcation criteria for the general model $\boldsymbol{B}_n + \boldsymbol{B}_s + \boldsymbol{B}_{to}$, Panel (a), the general $\mathcal{L}^M$ measure, defined by (18) and (19). Panel (b), the value of $\overline{Tw}$ for this system. At the nth bifurcation the value of $\overline{Tw}$ is in the range $(0.25 + 0.5(n-1), 0.25 + 0.5n)$, as indicated by the horizontal lines in panel (b). (Colour online)

But in this case we need to be careful with the definition of $\overline{Tw}$, more specifically the domain of integration used to calculate it. A simple example shows why. In the simpler straight separator model a current-carrying component of the field in the form

$$\boldsymbol{B}_{tc} = J(-y\hat{\boldsymbol{x}} + x\hat{\boldsymbol{y}}) + \frac{b_0}{L^2}(z_0^2 - z^2 + x^2 + y^2)\hat{\boldsymbol{z}}, \tag{20}$$

leads to a divergent mean twisting rate when evaluated on the separator, in the neighbourhood of the null's,

$$\overline{Tw}(\boldsymbol{x}_s) = \int_{-z_0}^{z_0} \frac{\boldsymbol{B}\cdot\nabla\times\boldsymbol{B}}{\boldsymbol{B}\cdot\boldsymbol{B}}\,\mathrm{d}z = \int_{-z_0}^{z_0} \frac{J}{z_0^2 - z^2}\,\mathrm{d}z,$$

and the integral itself is ill defined. This was not a problem in our exponentially decaying twisting models (at least at machine precision), but, as discussed above, the general separator geometry model we consider in this section has a non-zero current at the edge of the separator. We also would like to be able to deal with a model where there is a current in the form (20) and the prescription we detail here works in both cases.

This divergence in $\overline{Tw}$ is due to the rapid divergence of all neighbouring field lines from the null point. In the limit we approach the null the rate of this divergence becomes unbounded and, when there is current in the neighbourhood of the null, it leads to the observed divergence of $\overline{Tw}$. So we should be slightly wary of using the notation $\overline{Tw}$ to describe this quantity. It is only the mean twisting when the local field lines at one point on the separator remain within a local neighbourhood of the a separator, so that they can twist around the separator (a detailed investigation as to when it represents the twisting accurately in nonlinear force free extrapolations can be found in Liu *et al.* 2016).

We propose the following non-dimensionalised quantity to estimate when localised twisting is dominant

$$L\frac{\boldsymbol{B}\cdot\nabla\times\boldsymbol{B}}{\boldsymbol{B}\cdot\boldsymbol{B}}\bigg|_{\boldsymbol{x}=\boldsymbol{x}_s},$$

where L here is the arclength of the separator. As indicated, this is the fractional rate of twisting on the separator. If we make the reasonable assumption that the current is bounded

and not excessively large, then this will only diverge when tending towards a null $\boldsymbol{B}\cdot\boldsymbol{B}=0$ with a non zero current $\boldsymbol{B}\cdot\nabla\times\boldsymbol{B}$, exactly where the interpretation of this quantity as measuring twisting becomes invalid. Thus to measure twisting, we would want only to calculate the integral defining $\overline{Tw}(\boldsymbol{x}_s)$ when

$$L\frac{\boldsymbol{B}\cdot\nabla\times\boldsymbol{B}}{\boldsymbol{B}\cdot\boldsymbol{B}}\bigg|_{\boldsymbol{x}=\boldsymbol{x}_s}<C \tag{21}$$

for some constant C. This is relatively straightforward to calculate, so the aim is to make a sensible choice of C. For example, in figure 16 we see comparisons of $\mathcal{L}^m$ and $\overline{Tw}(\boldsymbol{x}_s)$ calculated with cut-offs $C=1,\ 10$ for the model

$$\frac{\mathrm{d}\theta}{\mathrm{d}z}=\frac{3z_0\sin(2\theta)+0.5+(2b_1/m)\exp(-z^2/l^2)}{z_0^2-z^2}. \tag{22}$$

The value $C=10$ is the length of the separator $L=10$ and the first just for comparison, there is a small reduction in twisting with the more strict constraint, but in both cases, the twisting gives the necessary bifurcation information, in that it is between $0.25n$ and $0.25n+0.5$ for each bifurcation.

In figure 17(b), we see a comparison of $\overline{Tw}$ to the bifurcations in the general system $\boldsymbol{B}_n+\boldsymbol{B}_s+\boldsymbol{B}_{to}$ under consideration in this section. We use the length of the separator for the value of the constant C to determine the integration domain of $\overline{Tw}$. We see that, for early bifurcations the $\overline{Tw}$ value is somewhat more of an overestimation than in previous cases, but that, for each bifurcation number n, its value is between $0.25+0.5(n-1)$ and $0.25+0.5n$, so retains its predictive capability when used in conjunction with $\mathcal{L}^m$.

5. Discussion

We have investigated criteria for current-induced separator bifurcation in a variety of systems, which are composed of a pair of null points and a separator curve that represents the fan plane intersection of the two separatrix surfaces. We have found the following accurate criterion to predict when these separators are close to bifurcating to form new separators.

5.1. The bifurcation predictor $\mathcal{L}^m$

First the quantity $\mathcal{L}^m$ the maximum linking of the local fan plane and the separator measured by comparison to its initial state. We showed that, if the quantity $\boldsymbol{B}\cdot\nabla\times\boldsymbol{B}$ is monotonic (or largely so) then $\mathcal{L}^m$ grows to a value of 0.25 when taken mod 0.25 then the separator is close to bifurcation and bifurcates when it reaches 0.25. The value of 0.25 is crucial as it means a field line emanating from the fan plane of the first null has rotated through a net angle $n\pi+\pi/2$ around the separator (relative to the separator rotation in the initial state). Every time this occurs, the separator crosses the fan plane of the second null point, thus altering the direction along the spine which the field line tends when it reaches the second null's local neighbourhood. To calculate the quantity, one takes the following

steps, which assume there is some initial state and then a sequence of states where the current at the null point is varied/increased:

- Identify the null points and the associated fan planes using standard methods (e.g.Haynes and Parnell 2007).
- Identify the separator field line $\boldsymbol{x}_s$ by mapping out the two fan surfaces, using bisection or a similar method to identify the start coordinates of the separator (x_{s0}, y_{s0}, z_0).
- Using an initial condition $(x_{s0}, y_{s0}, z_0) + \boldsymbol{\delta}$ with $\boldsymbol{\delta}$ a small vector which points along the fan plane, adjacent to the separator (here we use $|\delta| = 1 \times 10^{-8}$). Using this initial condition trace out a second field line $\boldsymbol{x}_{s\delta}$ which represents the local behaviour of the fan plane map in the neighbourhood $\boldsymbol{x}_s$.
- Split the field line curves $\boldsymbol{x}_s$ and $\boldsymbol{x}_{s\delta}$ into n points of even arclength spacing, which we label $\boldsymbol{x}_s^j$ and $\boldsymbol{x}_{s\delta}^j$. Then calculate $\mathcal{L}(\{\boldsymbol{x}_s^j\}_{j=1}^i, \{\boldsymbol{x}_{s\delta}^j\}_{j=1}^i)$, that is to say calculate the linking for all subsets of the full curves $\boldsymbol{x}_s$ and $\boldsymbol{x}_{s\delta}$.
- Calculate the maximum difference of these linking values from their values calculated on the initial field of the sequence. This maximum is $\mathcal{L}_m$.

A visual depiction and description of this calculation is given in figure 18 to complement the above description. We alert the reader to the fact code to calculate $\mathcal{L}(\boldsymbol{x}, \boldsymbol{y})$ for any pair of curves $(\boldsymbol{x}, \boldsymbol{y})$ is available in c++ at https://www.maths.dur.ac.uk/users/christopher.prior/code.html. A Mathematica version is also available on request.

We also highlight the fact that the choice of the initial point of field line $\boldsymbol{x}_{s\delta}$ is critical. In particular, it must satisfy the following two properties:

- The absolute value of δ needs to be small enough to genuinely capture the local behaviour of the separator, we would recommend the value suggested above.
- The second is that it should be on the fan surface of the initial null, or as close as possible. The reason for this is that if not, the null structure will almost immediately rotate the field line to lie along the fan plane (in the basic model (4) for example the term $\sin(2\theta)/(z_0^2 - z^2)$ does this when z is close to z_0). Thus there will be an in-built rotation which is not to do with the fan plane curves changing connectivity.

5.2. Mean twist and reversing currents

For situations where the current along the separator shows significant reversal, that is it has period of opposing sign of similar magnitudes, we can use the mean axial current

$$\overline{Tw}(\boldsymbol{x}) = \frac{1}{2\pi} \int_\gamma \frac{\boldsymbol{B} \cdot \nabla \times \boldsymbol{B}}{\boldsymbol{B} \cdot \boldsymbol{B}} \, \mathrm{d}s,$$

to predict when the (close to) bifurcation warnings given by the quantity $\mathcal{L}^m$ are correct. This quantity is related to the parallel current and in resistive MHD the parallel electric field. The integral of the latter is a measure of the reconnection rate of magnetic flux along the separator and is a commonly calculated quantity in studies of these structures. Typically $\overline{Tw}$ overestimates the total linkage (hence above 0.25) but also accounts for the current reversal where $\mathcal{L}^m$ does not, hence its use as an additional guide. The idea is that one only considers a bifurcation signal valid when:

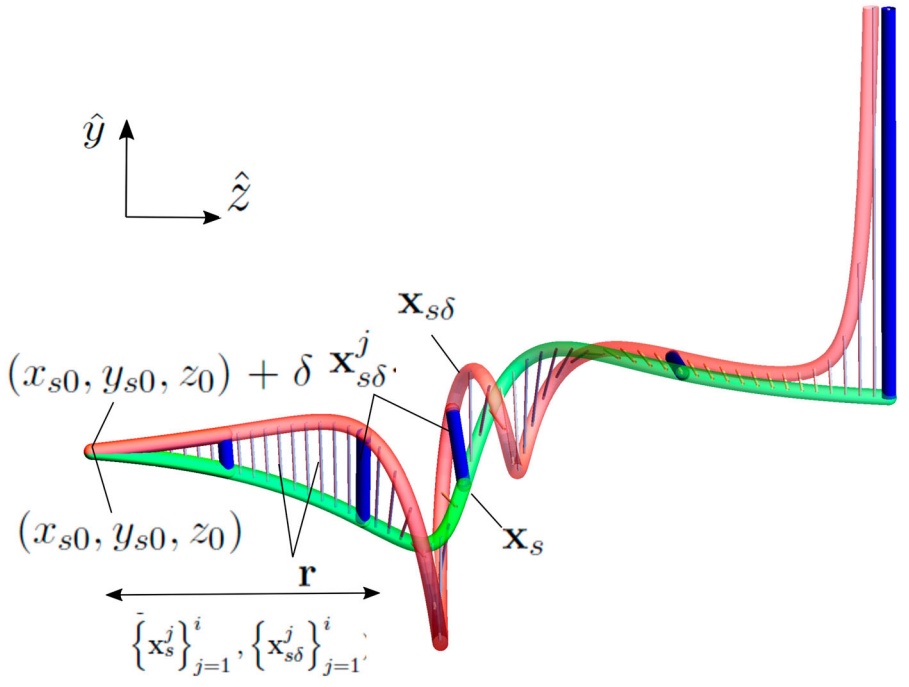

Figure 18. A visual depiction of the algorithm used the calculate $\mathcal{L}^m$ (note the $\hat{\boldsymbol{x}}$ direction is into the plane of view). The two launch points (x_{s0}, y_{s0}, z_0) and $(x_{s0}, y_{s0}, z_0) + \boldsymbol{\delta}$ are used to draw out the separator $\boldsymbol{x}_s$ and the curve $\boldsymbol{x}_{s\delta}$ used to estimate its local linear behaviour. The vector function $\boldsymbol{r}(z)$ whose rotation is used to calculate $\mathcal{L}(\boldsymbol{x}_s, \boldsymbol{x}_{s\delta})$ is shown. The curves are sampled at at a finite set of points $\boldsymbol{x}^j_s$ and $\boldsymbol{x}^j_{s\delta}$ whose joining vectors are shown by the blue vectors (note in practice we used a far finer discretisation ≈ 300 points). Then we create subset curves $(\{\boldsymbol{x}^j_s\}^i_{j=1}, \{\boldsymbol{x}^j_{s\delta}\}^i_{j=1})$ with these points, from the start of the pair up to a given j, as indicated by the double ended arrow at the bottom left of the figure. We calculate the linking for all of these subsets (there would be five such calculations in this figure). (Colour online)

- The value of $\bar{T}w$ is in the range $[0.25 + 0.5(n-1), 0.25 + 0.5n)]$ for the nth bifurcation.
- The bifurcation n has not already occurred, as we see in figure 9(d) $\mathcal{L}^m$ can still give bifurcation signals when $\bar{T}w$ is still in this range, but they do not indicate actual bifurcations.

We also found that $\mathcal{L}^m$ alone is a very accurate predictor of bifurcation when the current is highly axial. Condition (a) can be checked by seeing if the ratio of the axial current and the separator field strength remains bounded by some constant.

$$L \frac{\boldsymbol{B} \cdot \boldsymbol{\nabla} \times \boldsymbol{B}}{\boldsymbol{B} \cdot \boldsymbol{B}}\bigg|_{\boldsymbol{x}=\boldsymbol{x}_s} < C. \tag{23}$$

For example we found using C to be the length of the separator itself to be a sensible choice.

In future studies we aim to see how the winding $\mathcal{L}$ can be used to characterise other events such as the initial creation of separator structures and also whether it can be generalised to also characterise the bifurcation of Hyperbolic Flux Tubes for which a

similar process to separator bifurcation has recently been shown to occur (Wyper and Pontin 2021).

5.3. Separator annihilation

Finally, we note that throughout our analysis, we have assumed that the current at the original separator is growing via a progressive increase in the applied twist. This assumption is justifiable if the separator system is assumed to be subject to some external forcing such as flux emergence (Parnell *et al.* 2010) or the impact of the solar wind on the day side magnetosphere (Dorelli and Bhattacharjee 2009), and indeed the bifurcations and changes in topology are identical. However, if such forcing is removed, the system will relax with the current in the system reduced via reconnection. In this case, any separators previously formed via bifurcations will annihilate in pairs, reversing the bifurcation process by which they formed. Such a scenario is simply modelled in our previous examples by considering how the linking changes as the twist parameter is reduced, e.g. how $\mathcal{L}^m$ changes from right to left in figure 8. This gives one further prediction: in a relaxing separator system a reduction of $\mathcal{L}^m$ to 0 mod 0.25 corresponds to a separator pair imminently annihilating. Separator annihiliation would require the absolute value of the winding decrease $|\mathcal{L}(t)| < |\mathcal{L}_0|$, indicating the surfaces become unwound due to reconnection (and vice versa for separator creation).

Disclosure statement

No potential conflict of interest was reported by the author(s).

ORCID

C. Prior http://orcid.org/0000-0003-4015-5106

References

Aslanyan, V., Pontin, D.I., Wyper, P.F., Scott, R.B., Antiochos, S.K. and DeVore, C.R., Effects of pseudostreamer boundary dynamics on heliospheric field and wind. *Astrophys. J.* 2021, **909**, 10.

Aulanier, G., Pariat, E. and Démoulin, P., Current sheet formation in quasi-separatrix layers and hyperbolic flux tubes. *Astron. Astrophys.* 2005, **444**, 961–976.

Berger, M.A. and Prior, C., The writhe of open and closed curves. *J. Phys. A Math. Theor.* 2006, **39**, 8321.

Dorelli, J.C. and Bhattacharjee, A., On the generation and topology of flux transfer events. *J. Geophys. Res. (Space Phys.)* 2009, **114**, A06213.

Glocer, A., Dorelli, J., Toth, G., Komar, C. and Cassak, P., Separator reconnection at the magnetopause for predominantly northward and southward IMF: techniques and results. *J. Geophys. Res. (Space Phys.)* 2016, **121**, 140–156.

Haynes, A.L. and Parnell, C.E., A trilinear method for finding null points in a three-dimensional vector space. *Phys. Plasmas* 2007, **14**, 082107.

Haynes, A.L., Parnell, C.E., Galsgaard, K. and Priest, E.R., Magnetohydrodynamic evolution of magnetic skeletons. *Proc. Math. Phys. Eng.* 2007, **463**, 1097–1115.

Hesse, M. and Schindler, K., A theoretical foundation of general magnetic reconnection. *J. Geophys. Res.* 1988, **93**, 5559–5567.

Hornig, G. and Priest, E., Evolution of magnetic flux in an isolated reconnection process. *Phys. Plasmas* 2003, **10**, 2712–2721.

Liu, R., Kliem, B., Titov, V.S., Chen, J., Wang, Y., Wang, H., Liu, C., Xu, Y. and Wiegelmann, T., Structure, stability, and evolution of magnetic flux ropes from the perspective of magnetic twist. *Astrophys. J.* 2016, **818**, 148.
MacTaggart, D. and Haynes, A.L., On magnetic reconnection and flux rope topology in solar flux emergence. *Mon. Not. R. Astron. Soc.* 2014, **438**, 1500–1506.
Parnell, C., Smith, J., Neukirch, T. and Priest, E., The structure of three-dimensional magnetic neutral points. *Phys. Plasmas* 1996, **3**, 759–770.
Parnell, C.E., Haynes, A.L. and Galsgaard, K., Recursive reconnection and magnetic skeletons. *Astrophys. J.* 2008, **675**, 1656–1665.
Parnell, C.E., Haynes, A.L. and Galsgaard, K., Structure of magnetic separators and separator reconnection. *J. Geophys. Res. (Space Phys.)* 2010, **115**, A02102.
Parnell, C.E., Maclean, R.C. and Haynes, A.L., The detection of numerous magnetic separators in a three-dimensional magnetohydrodynamic model of solar emerging flux. *Astrophys. J.* 2010, **725**, L214–L218.
Pontin, D. and Wyper, P., The effect of reconnection on the structure of the Sun's open-closed flux boundary. *Astrophys. J.* 2015, **805**, 39.
Priest, E. and Forbes, T., *Magnetic Reconnection*, 2000 (Cambridge University Press: New York).
Priest, E.R. and Pontin, D.I., Three-dimensional null point reconnection regimes. *Phys. Plasmas* 2009, **16**, 122101.
Priest, E.R. and Titov, V.S., Magnetic reconnection at three-dimensional null points. *Proc. R. Soc. Lond. A* 1996, **354**, 2951–2992.
Priest, E.R., Lonie, D.P. and Titov, V.S., Bifurcations of magnetic topology by the creation or annihilation of null points. *J. Plasma Phys.* 1996, **56**, 507–530.
Stevenson, J.E.H., Parnell, C.E., Priest, E.R. and Haynes, A.L., The nature of separator current layers in MHS equilibria-I. Current parallel to the separator. *Astron. Astrophys.* 2015, **573**, A44.
Wilmot-Smith, A. and Hornig, G., A time-dependent model for magnetic reconnection in the presence of a separator. *Astrophys. J.* 2011, **740**, 89.
Wyper, P.F. and Hesse, M., Quantifying three dimensional reconnection in fragmented current layers. *Phys. Plasmas* 2015, **22**, 042117.
Wyper, P. and Pontin, D., Dynamic topology and flux rope evolution during non-linear tearing of 3D null point current sheets. *Phys. Plasmas* 2014, **21**, 102102.
Wyper, P.F. and Pontin, D.I., Is flare ribbon fine structure related to tearing in the flare current sheet? *Astrophys. J.* 2021, **920**, 102.
Wyper, P.F., Antiochos, S.K., DeVore, C.R., Lynch, B.J., Karpen, J.T. and Kumar, P., A model for the coupled eruption of a pseudostreamer and helmet streamer. *Astrophys. J.* 2021, **909**, 54.
Yang, S., Zhang, Q., Xu, Z., Zhang, J., Zhong, Z. and Guo, Y., Imaging and spectral study on the null point of a fan-spine structure during a solar flare. *Astrophys. J.* 2020, **898**, 101.
Zhu, X. and Wiegelmann, T., Testing magnetohydrostatic extrapolation with radiative MHD simulation of a solar flare. *Astron. Astrophys.* 2019, **631**, A162.
Zweibel, E.G. and Yamada, M., Magnetic reconnection in astrophysical and laboratory plasmas. *Annu. Rev. Astron. Astrophys.* 2009, **47**, 291–332.

Appendix. The net winding $\mathcal{L}$ of arbitrary curves

For general curves $\boldsymbol{x}$ and $\boldsymbol{y}$, we define a vector $\boldsymbol{r} = \boldsymbol{y}(z) - \boldsymbol{x}(z)$ where both curves have the same z coordinate. We then define

$$\Theta(z) = \arctan\left(\frac{\boldsymbol{r}\cdot\hat{\boldsymbol{y}}}{\boldsymbol{r}\cdot\hat{\boldsymbol{x}}}\right),$$

so that

$$\frac{\mathrm{d}\Theta}{\mathrm{d}z} = \frac{\hat{\boldsymbol{z}}\cdot(\boldsymbol{r}\times\mathrm{d}\boldsymbol{r}/\mathrm{d}z)}{\boldsymbol{r}\cdot\boldsymbol{r}}.$$

Then we have

$$\mathcal{L}(\boldsymbol{x}, \boldsymbol{y}) := \frac{1}{2\pi} \int_{-z_0}^{z_0} \frac{\mathrm{d}\Theta}{\mathrm{d}z} \, \mathrm{d}z.$$

To deal with curves whose height function is multi-valued, we split the curve via its *turning points* for which $\mathrm{d}x_z/\mathrm{d}z$. We mark each curve as rising or falling,

$$\sigma(\boldsymbol{x}_i) = \begin{cases} 1 & \text{if} \quad \mathrm{d}x_z/\mathrm{d}z > 0, \\ -1 & \text{if} \quad \mathrm{d}x_z/\mathrm{d}z < 0. \end{cases}$$

Then we have

$$\mathcal{L}(\boldsymbol{x}, \boldsymbol{y}) := \sum_{i=1}^{n+1} \sum_{j=1}^{m+1} \frac{\sigma(\boldsymbol{x}_i)\sigma(\boldsymbol{y}_j)}{2\pi} \int_{z_{ij}^{\min}}^{z_{ij}^{\max}} \frac{\mathrm{d}\Theta(\boldsymbol{x}_i(z), \boldsymbol{y}_j(z))}{\mathrm{d}z} \, \mathrm{d}z,$$

where $z_{ij}^{\min}$, $z_{ij}^{\max}$ is the mutual z range of sections of curve $\boldsymbol{x}_i$ and $\boldsymbol{y}_j$ (Berger and Prior 2006). This is valid for combinations of curve which span the planes, are anchored on both planes and are closed in the domain.